

See discussions, stats, and author profiles for this publication at: <https://www.researchgate.net/publication/320802229>

Surface functionalized UiO-66/Pebax-based ultrathin composite hollow fiber gas separation membranes

Article in *Journal of Materials Chemistry A* · November 2017

DOI: 10.1039/C7TA07512J

CITATIONS

6

READS

141

8 authors, including:



Putu Doddy Sutrisna

Universitas Surabaya

17 PUBLICATIONS **144** CITATIONS

[SEE PROFILE](#)



Jingwei Hou

University of Cambridge

61 PUBLICATIONS **802** CITATIONS

[SEE PROFILE](#)



Hongyu Li

UNSW Sydney

55 PUBLICATIONS **1,335** CITATIONS

[SEE PROFILE](#)

Some of the authors of this publication are also working on these related projects:



biofouling alleviation of PES UF MMM [View project](#)



Aligned membrane for water treatment and gas separation. [View project](#)



Cite this: DOI: 10.1039/c7ta07512j

Surface functionalized UiO-66/Pebax-based ultrathin composite hollow fiber gas separation membranes†

Putu Doddy Sutrisna,^a Jingwei Hou,^b Muhammad Yazid Zulkifli,^a Hongyu Li,^a Yatao Zhang,^c Weibin Liang,^d Deanna M. D'Alessandro^d and Vicki Chen^a

Pebax-based composite hollow fibre membranes are promising candidates for industrial gas separation, but their application is limited by the inherent separation performance of the polymeric materials and the poor operational stability especially under elevated pressures. The incorporation of metal–organic frameworks (MOFs) has been extensively investigated as a potential solution to these problems. However, the major challenges are to control the microvoids in the interfacial region and to improve the effective MOF loading within the selective layer. In this work, we applied a zirconium-based rigid MOF (UiO-66) to fabricate a nanocomposite hollow fibre membrane, and (–COOH) and (–NH₂) modified UiO-66 were applied to investigate the effect of surface functionalization. Up to 80 wt% UiO-66 was incorporated into the thin Pebax selective layer, and both improved CO₂ permeance and selectivity were obtained simultaneously with the (–NH) functionalized UiO-66. In addition, the presence of UiO-66 in Pebax significantly improved the membrane's operational stability under high pressure.

Received 25th August 2017
Accepted 1st November 2017

DOI: 10.1039/c7ta07512j

rsc.li/materials-a

1 Introduction

Membrane-based gas separation processes are flexible, easy to operate and scale up, and require smaller footprints. They have therefore been the subject of considerable research attention, especially for CO₂ capture from flue gas and natural gas sweetening.^{1–3} Polymeric membranes are considered as the most promising candidate for industrial application, yet their application is limited by the inherent performance of the polymeric materials and poor operational stability, especially under high pressure. To tackle these problems, different nanofillers have been incorporated into the polymeric matrix to fabricate mixed matrix membranes (MMMs). Recently, metal–organic frameworks (MOFs) have been extensively investigated for gas adsorption and separation.^{4,5} MOFs are heralded for their chemical and structural versatility in being able to accommodate an enormous amount of functionalities: molecular sieve pores can be effectively incorporated into polymeric materials to promote the separation performance.^{4,6,7} Some

MMMs have their performance surpassing the Robeson upper bound which depicts the gas permeability–selectivity trade-off for pure polymeric materials.^{8–13}

Currently, most MMMs are synthesized as dense flat sheets.^{14–20} These membranes, from the material's perspective, can have superior permeability. Yet this does not necessarily indicate that the membrane can readily achieve high permeation flux (permeance), which is of higher practical importance. For gas separation membranes, the thickness does matter. Ideally, hollow fiber composite membranes with large surface areas and thin selective layers are preferred.²¹ However, the behaviour of MOF–polymer membranes in their thin film can be different from that of their bulkier, thick counterparts. This is due to the difficulty in achieving a homogeneous MOF dispersion and a higher possibility of generating extra non-selective defects. In addition, the polymer chain rigidification effect caused by interfacial interaction can be more significant.²² Among different MOF materials, ZIF-8 has been extensively investigated due to its small pore size (3.4 Å) and reasonably good chemical stability.^{23,24} In one of our previous studies, the introduction of in-house synthesized ZIF-8 into a thin Pebax layer clearly generated extra defects due to the poor compatibility in the interfacial region, and the loss of gas selectivity was more significant for the thin selective layer on the hollow fiber composite membranes compared with thick mixed matrix membranes.²⁵ To tackle this problem, polydopamine modification has been carried out to fine-tune the interfacial compatibility: compared with the pristine ZIF-8, the membranes with modified ZIF-8 exhibited improved gas

^aUNESCO Centre for Membrane Science and Technology, School of Chemical Engineering, University of New South Wales, Sydney, NSW 2052, Australia. E-mail: jingwei.hou@unsw.edu.au

^bDepartment of Materials Science and Metallurgy, University of Cambridge, Cambridge, CB3 0FS, UK

^cSchool of Chemical Engineering and Energy, Zhengzhou University, Zhengzhou 450001, PR China

^dSchool of Chemistry, The University of Sydney, Sydney, NSW 2006, Australia

† Electronic supplementary information (ESI) available. See DOI: 10.1039/c7ta07512j

selectivity, which however were still lower than that of the original pure polymer membrane.¹⁵

Recent studies have started to shed light on the mechanical properties of MOFs.²⁶ Among different MOF materials, ZIF-8 has a low elastic modulus and hardness, indicating its good elasticity in the family of crystalline materials. We also first demonstrated that a thin, continuous ZIF-8 membrane can maintain a certain degree of flexibility: it can sustain bending and elongation without compromising its molecular sieving capability.⁵ The rotational and vibrational movement of the imidazole linkers in the ZIF has also been experimentally demonstrated by Terahertz FTIR with synchrotron beamlines.²⁷ This interesting property, however, may compromise their inherent molecular sieving capability based on their crystalline framework structures.²⁸ As a result, the incorporation of such “soft” MOFs into the thin composite membrane can potentially lead to the formation of non-selective interfacial microvoids, or its flexible framework structure can allow the passage of gas molecules which are larger than its pore aperture.²⁹ This problem can potentially be solved by blending more rigid MOFs into the membrane. Another problem for the MOF-containing membranes is their relatively low MOF loading, as aggregation of the particles at high concentration (over 30 wt%) can create defects in membranes: for most existing nanocomposite membranes, only up to 30 wt% of MOFs can be achieved without significant deterioration in the selectivity.^{17–19,30}

In this study, we fabricate our composite membrane with different types of MOFs, namely University of Oslo-66 (UiO-66) and zeolitic imidazolate framework-7 (ZIF-7). UiO-66 ($[\text{Zr}_6\text{O}_4(\text{OH})_4(\text{bdc})_6]$ where bdc = 1,4-benzenedicarboxylate) is considered as one of the most rigid MOFs due to the high degree of coordination of the Zr–O node to organic ligands.³¹ Its structure is comprised of a central octahedral cage with 8 face-sharing super-tetrahedra (ST). The four vertices of the ST are each occupied by a Zr₆-oxo cluster with edges formed by the bdc ligands.³² Its satisfactory thermal and chemical stabilities over a wide range of temperature and pH make it a suitable candidate for membrane application, both as a filler and a coherent selective layer.^{33–35} In addition, by substituting the bdc ligand with other linear dicarboxylate linkers, a series of isorecticular frameworks with different cavity sizes and functionalities can be obtained (Scheme 1). Enhancement in the gas separation

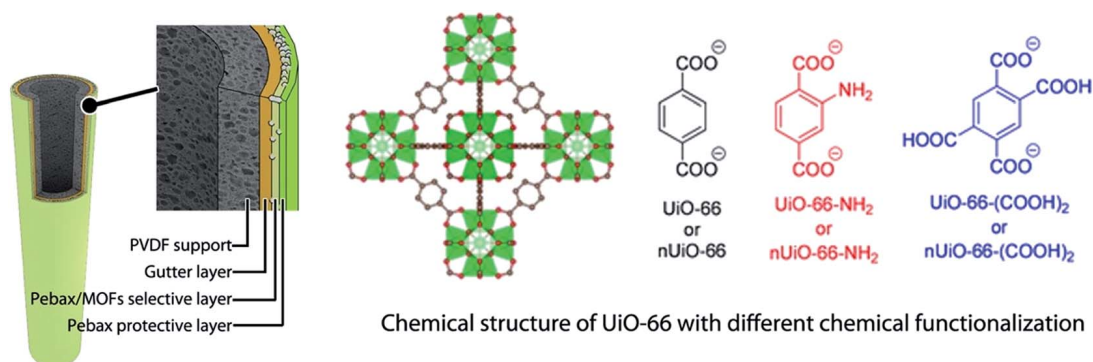
performance in the presence of functional groups such as amine on UiO-66/Pebax flat sheet mixed matrix membranes has also been reported,³⁰ but their effect on the composite membrane performance has never been investigated. Another targeted MOF is ZIF-7 ($[\text{Zn}(\text{BIm})_2]$ where BIm = 2-benzimidazolate) which has an aperture size of ~ 3.0 angstroms, smaller than that in ZIF-8 (~ 3.4 angstroms). Although ZIF-7 possesses a similar structure to ZIF-8, it has higher rigidity.²⁶ Thus, ZIF-7 is considered to be an appropriate candidate to investigate the effect of the structural rigidity of a MOF on the membrane performance, and a direct comparison can be made against ZIF-8.

In this work, UiO-66, UiO-66-NH₂, UiO-66-(COOH)₂ and ZIF-7 were incorporated into the thin Pebax selective layer of composite hollow fiber membranes. The copolymer Pebax, which features a hard polyamide (PA) segment and a soft polyethylene oxide (PEO) segment, has shown good performance for CO₂ gas separation and has exhibited plasticization resistance to CO₂ gas. The interaction between the copolymer and MOF additives can be complex and therefore warrants detailed investigation. Membranes containing up to 80 wt% of UiO-66 and 30 wt% of ZIF-7 were examined to understand their effect on the CO₂, N₂ and CH₄ permeances. Both pure gas and mixed gases were investigated. In addition, a complete pressurization–depressurization cycle was applied to investigate the effect of MOFs on the membrane plasticization and compaction resistance.

2 Materials and methods

2.1 Materials

Hollow fiber PVDF porous membranes were kindly supplied by Beijing OriginWater Technology Co., Ltd. (China) with a diameter of 1.0 mm, a wall thickness of 0.25 mm and a pore size of ~ 0.05 μm . Poly[1-(trimethylsilyl)prop-1-yne] (PTMSP) utilized as the gutter layer was provided by Gelest, Inc., PA, USA. Polyether oxide–polyamide (PEO–PA) blocks (Pebax-1657) supplied by Arkema, France were used as the polymer matrix for the selective layer. The Pebax-1657 applied in this work contained 60% rubbery PEO phase and 40% glassy PA phase. Chemicals for ZIF-7 and UiO-66 particle synthesis were supplied by Sigma-Aldrich, including benzimidazole, zinc nitrate hexahydrate (for ZIF-7), ZrCl₄ (>99.5%), and ligands (H₂bdc (1,4-benzenedicarboxylic acid, 98%)



Scheme 1 Schematic diagram of the composite membrane and the chemical structure of UiO-66.

for UiO-66, H₂bdc-NH₂ (2-amino-1,4-benzendicarboxylic acid, 99%) for UiO-66-NH₂, and H₂bdc-(COOH)₂ (1,2,4,5-benzenetetracarboxylic acid, 96%) for UiO-66-(COOH)₂. Hydrochloric acid (HCl, 32%) and *N,N*-dimethylformamide (DMF, > 98%) were obtained from Merck. CO₂, CH₄ and N₂ pure gases and mixed gases (CO₂/N₂, 20 : 80 v/v and CO₂/CH₄, 20 : 80 v/v) for the gas permeation test were purchased from Coregas. All other chemicals were used without further purification.

2.2 Synthesis of UiO-66 and ZIF-7 particles

ZIF-7 particles were synthesized at room temperature as described elsewhere with slight modification.^{36,37} In a typical procedure, a mixture of 0.453 g zinc nitrate hexahydrate, 1.154 g benzimidazole and 150 ml DMF was stirred for 24 h at room temperature. The milky solution was subsequently centrifuged for 15 min at 13 000 rpm. ZIF-7 particles were then washed and centrifuged with DMF for another 2 cycles, before being washed with methanol for another 24 h to remove DMF. The final product of the ZIF-7 particles was recovered by centrifugation and mixed with an ethanol/water mixture (70/30 w/w or 74.7/25.3 v/v) for membrane fabrication. For the particle characterization, the particles were dried for 24 h at 85 °C.

The UiO-66 and functionalized UiO-66 particles were synthesized by microwave-assisted synthesis using an Anton Paar Monowave 300 microwave oven.^{38,39} A 30 ml glass microwave vial was filled with ZrCl₄ and the appropriate ligand, H₂bdc (1,4-benzendicarboxylic acid) for UiO-66, H₂bdc-NH₂ (2-amino-1,4-benzendicarboxylic acid) for UiO-66-NH₂, and H₂bdc-(COOH)₂ (1,2,4,5-benzene tetracarboxylic acid) for UiO-66-(COOH)₂. Thereafter, concentrated HCl, formic acid and DMF were introduced into the vial. The mixture was heated with magnetic stirring (600 rpm) to 160 °C within 30 min and held at this temperature for 40 min before the final cooling to 55 °C. The precipitates were obtained by vacuum filtration and repeatedly washed with DMF (3 × 20 ml) and acetone (5 × 20 ml). The materials were subsequently solvent exchanged with methanol using a Soxhlet washing procedure for 10 h. The resulting powders were dried under vacuum. The yields for UiO-66 were as follows: UiO-66: 88.9%, UiO-66-NH₂: 91.0% and UiO-66-(COOH)₂: 90.3%.

2.3 Fabrication of hollow fiber nanocomposite membranes

In this work, supporting PVDF membranes with relatively large pores were selected to ensure high mass transfer efficiency. To mitigate the coating layer intrusion into the pores, the PVDF membranes were firstly soaked overnight in deionized (DI) water and then briefly wiped with a paper tissue to remove the water on the membrane surface, but leaving the membrane pores occupied with water. Both ends of the fibers were clamped with longtail clips to prevent coating solution intrusion into the lumen side during the dip coating process. The outer surface of fibers was firstly dip-coated with a highly permeable gutter layer four times using 2 wt% PTMSP in *n*-hexane solution. The smooth surface can facilitate the subsequent coating of a thin and continuous selective layer. The selective layer of the

MOFs/Pebax-1657-based composite membrane was prepared by dispersing nanoparticles in Pebax solution (3 wt% Pebax in 70/30 w/w ethanol/water). Two coating cycles were applied for the selective layer. Finally, a pure Pebax-1657 layer was coated as a protective layer to seal any possible defects.

To ensure good MOF dispersion, the particles were first primed with the Pebax-1657 solution. Then the mixture was probe sonicated. For the dip-coating procedure, the fibers were turned upside down after each coating cycle and dried in an oven at 50 °C. More details of the dip-coating procedure can be found in our previous publication.²⁵ For the subsequent gas permeation tests, three hollow fibers were housed in a 1/4 inch and 18 cm long stainless steel module with an effective membrane area of 17 cm².

2.4 Characterization of the nanoparticles and membranes

ZIF-7 and UiO-66 particles were analyzed using a Transmission Electron Microscope (TEM), FEI Tecnai G2 20, for imaging purposes. The particle size was monitored using a dynamic light scattering (DLS) device (Malvern Nano DLS). For each test, at least 13 cycles of reading were performed to minimize error. The Brunauer–Emmett–Teller (BET) surface area, Barrett–Joyner–Halenda (BJH) pore volume, and N₂ and CO₂ sorption isotherms were recorded on an Accelerated Surface Area and Porosimetry System, ASAP 2020 (Micromeritics Instruments Inc.). Approximately 80 mg of the powdered solid was loaded into a glass analysis tube and dehumidified for 3 h under dynamic vacuum at 150 °C. N₂ adsorption and desorption isotherms were measured at 77 K while CO₂ adsorption and desorption isotherms were measured at 298.15 K. The chemical structure of the particles was analyzed using a Fourier Transform Infra-Red (FTIR) Alpha spectrometer from 400 to 4000 cm⁻¹. The crystallinity of the particles was examined using a PANalytical Empyrean Thin-Film X-Ray Diffraction (XRD) instrument in the 2θ range from 4 to 36° with a 0.026° step size.

Characterization of the composite membranes was conducted using Scanning Electron Microscopy (SEM), Energy Dispersive X-ray (EDX) analysis, Differential Scanning Calorimetry (DSC), FTIR and XRD techniques. The surface and cross-sectional areas of the membranes were examined under an FEI Nova NanoSEM 450 FESEM after the membrane sample was coated with a layer of chromium. The presence of nanoparticles and the quality of dispersion in the membrane matrix were examined by EDX line scans (FEI Nova NanoSEM 450 FESEM). The samples were coated with a layer of carbon prior to the EDX tests. The degree of crystallinity of the membranes was determined by DSC analysis. The Pebax-based membranes were tested with a Mettler Toledo DSC 823e analyzer from -30 °C to 400 °C in two cycles. The crystallinity of the membranes was analyzed using a PANalytical Empyrean Thin-Film XRD instrument in the 2θ range from 4 to 36° with a 0.026° step size. The chemical structure of the membranes was analyzed using a Fourier Transform Infra-Red (FTIR) Alpha spectrometer from 400 to 4000 cm⁻¹. Tensile strength tests were carried out with a textural analyzer (TAXT2, Stable Micro Systems). The sample length was 100 mm and the testing speed was 0.5 mm s⁻¹.

2.5 Gas permeation testing

The gas permeation tests using pure gas and mixed gases to measure the initial performance of the membrane were carried out at room temperature (around 25 °C). The volumetric flow rate of the permeate line was measured using a bubble flow meter for low permeate flow rates (<1 ml min⁻¹), while flow rates higher than 1 ml min⁻¹ were recorded using an Agilent ADM1000 gas flow meter. The pure gas permeance was calculated using eqn (1):

$$\frac{P}{l} = \frac{Q}{A\Delta p} \quad (1)$$

where P/l is the gas permeance through the membrane, Q is the volumetric flow rate of the permeate line (ml s⁻¹), Δp is the pressure difference across the membrane (cm Hg), and A is the membrane surface area (cm²).

The ideal selectivity of the membrane for a given gas pair was calculated from the ratio of the permeance of fast gas (A) to that of slow gas (B) based on eqn (2):

$$\alpha = \frac{(P/l)_A}{(P/l)_B} \quad (2)$$

The operational stability of the composite membranes was studied under different feed pressures. The experiments were conducted by exposing the membranes to different feed pressures in a full pressurization–depressurization cycle from 2 to 15 bar. The feed gas pressure was increased and decreased stepwise. Under each pressure, the membrane was exposed to the feed gas for 1 hour for sufficient equilibration. The permeability of CO₂ was firstly tested, followed by a CH₄ test to understand the effect of the condensable gas on the permeation behavior of the non-condensable gas.

To study the effect of competitive sorption during gas permeation, mixed gas permeation tests were also carried out using CO₂/CH₄ and CO₂/N₂ (20/80, v/v) gas mixtures as feeds. The permeate composition was analyzed with a Shimadzu gas chromatograph (Shimadzu GC-2014) using a TCD and the mixed-gas permeability was calculated using eqn (3):

$$\frac{P}{l} = \frac{QY_A}{A(p_x X_A - p_y Y_A)} \quad (3)$$

where p_x and p_y are the pressures of the feed and permeate, A is the membrane area, and X and Y are the concentrations in the feed and permeate sides. The selectivity of the membrane for mixed gases was calculated using eqn (4):^{40,41}

$$\alpha_B^A = \frac{Y_A/Y_B}{(p_x X_A - p_y Y_A)/(p_x X_B - p_y Y_B)} \quad (4)$$

3 Results and discussion

3.1 Characterization of UiO-66 and ZIF-7 particles

The morphologies of UiO-66 and ZIF-7 nanoparticles were examined by TEM (Fig. 1). Both UiO-66 and functionalized UiO-66 showed rectangular shapes with particle sizes of around

100–200 nm, which aligns with the DLS results in Table 1. This observation suggests that the different organic ligands did not change the crystal structure or particle sizes of UiO-66. This is preferable to help us understand the effect of the intrinsic MOF properties, rather than the particle size and crystalline structure, on the final composite membrane performance. In terms of the ZIF-7 nanoparticles, the morphology of such particles showed a rhombic dodecahedral shape with a particle size of around 150 nm. Such an observation is consistent with previous literature.³⁷

The particles were analyzed for their BET surface area, BJH pore volume and adsorption average pore diameter, with the results presented in Table 1. The ZIF-7 synthesized in this research had a BET surface area of around 469 m² g⁻¹, which is in agreement with a previous study.³⁷ The surface area of ZIF-7 was smaller than that of ZIF-8 reported previously,²⁵ possibly due to the smaller accessible window apertures in ZIF-7 (~3.0 angstroms) compared with ZIF-8 particles (~3.4 angstroms). The BET surface area of UiO-66 particles was around 1800 m² g⁻¹. The high surface area confirmed the effectiveness of the solvent exchange process during particle synthesis. The BET surface area, BJH pore volume and pore diameter of the UiO-66 were higher than those of the functionalized UiO-66. This is consistent with the presence of functional groups on the organic ligands which partially block the pores in UiO-66.^{42,43} Particles with the bulkier -(COOH)₂ functional group showed the smallest BET surface area and BJH pore volume among all the UiO-66 derivatives.

To further explore the effect of functional groups on the UiO-66 gas adsorption process, the adsorption–desorption isotherms were investigated for both N₂ and CO₂ (Fig. 2). Functionalization of the organic ligands has two effects: on the

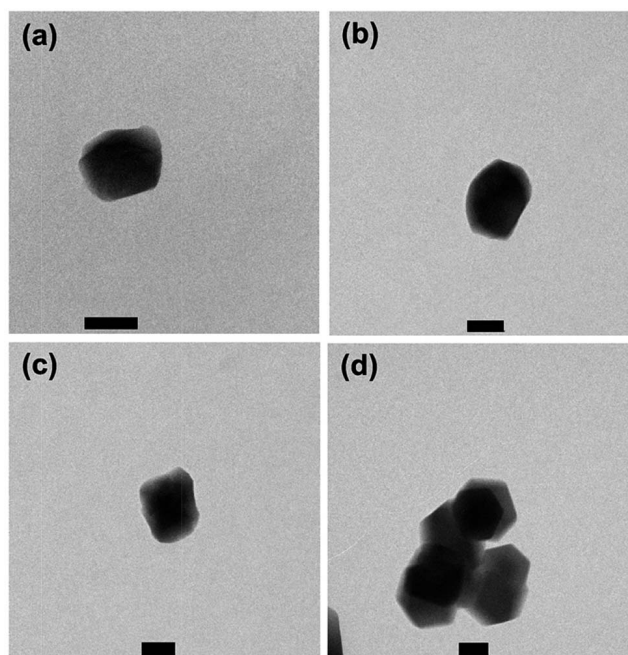


Fig. 1 TEM images of (a) UiO-66, (b) UiO-66-NH₂, (c) UiO-66-(COOH)₂ and (d) ZIF-7. The scale bar is 100 nm.

Table 1 Average particle size, BET surface area and BJH pore volume of various UiO-66 and ZIF-7 particles

Type of particle	DLS results (nm)	BET surface area (m ² g ⁻¹)	BJH pore volume (cm ³ /g ⁻¹)	Adsorption average pore diameter (nm)
UiO-66	130 ± 15	1800 ± 2.5	0.68	1.5
UiO-66-NH ₂	146 ± 15	1213 ± 6	0.48	1.45
UiO-66-(COOH) ₂	150 ± 10	400 ± 0.8	0.17	1.33
ZIF-7	171 ± 13	469 ± 2	0.39	1.12

one hand, it could reduce the UiO-66 pore size and lead to a reduced BET surface area as discussed above. For the -COOH functionalized MOFs, each organic ligand contains two -COOH groups, leading to significant pore blockage and subsequently low adsorption capacity. On the other hand, the presence of polar moieties such as -NH₂ can improve the adsorption capacity for CO₂, resulting in the highest CO₂ adsorption for UiO-66-(NH₂), even though its surface area is smaller than that of UiO-66.

The chemical properties of the MOFs synthesized in this research were analyzed using FTIR analysis and the results are presented in Fig. S1.† The FTIR spectra of UiO-66 and its derivatives show a weak band at 1660 cm⁻¹, which was assigned to the stretching vibrations of C=O in the carboxylic acid present in the bdc ligand. The asymmetric stretching vibration observed at around 1585 cm⁻¹ originated from O-C-O asymmetric stretching in the bdc ligand. The vibration of C=C in the benzene ring can be observed at 1506 cm⁻¹ and the O-C-O symmetric stretching vibration in the carboxylate group of the bdc ligand was observed as a small band at 1395 cm⁻¹.^{44,45} For UiO-66-NH₂, the presence of primary amino functional groups (N-H) was confirmed by the small peaks at 3367 and 3475 cm⁻¹.⁴⁶ The peak at 1710 cm⁻¹ for UiO-66-(COOH)₂ is consistent with a free carboxylic acid C=O stretching vibration.⁴⁷ For ZIF-7 particles, signature peaks at 1455 and 750 cm⁻¹ were observed in Fig. S1c,† corresponding to the C=C and C-H bonds in the benzene functional group of benzimidazole as the organic ligand.⁴⁸

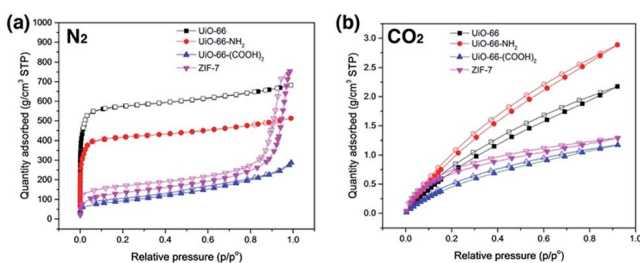


Fig. 2 (a) N₂ and (b) CO₂ adsorption for UiO-66 derivatives and ZIF-7 particles. The filled symbols represent adsorption and the open symbols represent desorption. N₂ adsorption and desorption isotherms were measured at 77 K while CO₂ adsorption and desorption isotherms were measured at 298.15 K. Both measured pressures were up to 1 bar.

XRD analysis was then carried out to investigate the crystallinity of the UiO-66 and ZIF-7 particles as shown in Fig. S2.† In terms of UiO-66 and its derivatives, the XRD pattern of UiO-66 in Fig. S2a† shows signature peaks at $2\theta = 7.28^\circ$, 8.42° and 25.63° . These were in accordance with the peak positions observed in other studies on UiO-66 particle synthesis.⁴⁹ After the incorporation of the amine -(NH₂) and -(COOH)₂ functionalities, the positions of the peaks were largely invariant. This indicates the preservation of crystallinity of the UiO-66 particles despite the change in chemical moieties on the organic ligands. The crystallinity of ZIF-7 was confirmed from the powder X-ray diffraction patterns shown in Fig. S2b.† The pattern aligned well with literature values.³⁷

3.2 Characterization of UiO-66/Pebax-based hollow fiber composite membranes

The performance of the composite membrane is determined by the intrinsic properties of the materials as well as the interfacial interactions.⁵⁰ In this work, the composite membranes consisted of a PVDF porous support, a layer of PTMSP as a gutter layer, a Pebax-1657-based selective layer (containing different amounts of MOFs) and a top pure Pebax-1657 protective layer. Each of these layers contributes to the overall gas separation performance of the membranes.

3.2.1 Morphology of the composite membranes. Firstly, we examined the membrane cross-sectional morphology. As shown in Fig. 3, the thickness of the PTMSP gutter layer was approximately 6 to 7 μm. This is the optimum thickness that can ensure even and uniform coverage of the PVDF support as has been investigated in our previous study.²⁵ Uniform and continuous coverage of the porous support with PTMSP will prevent the intrusion of the selective layer into the pores of the porous support, ensuring an even and thin selective layer for higher permeation flux.

The further deposition of a selective layer and a protective layer increased the thickness of the membranes by around 1–1.5 μm. However, the distinct boundary between the gutter and selective layers cannot be observed clearly under a SEM due to the interfusion between these two layers. This has also been observed in our previous study.²⁵ It was difficult to obtain high-resolution cross-sectional images of the nanocomposite hollow fiber membranes: due to the poor conductivity of the porous substrates and their tubular shape, a significant electron beam drifting can occur at high magnification. Based on the SEM images presented here, the presence of UiO-66 (Fig. 3c–e) can be observed in the top region of the composite membrane (as highlighted in the images). When the UiO-66 loading was at 80 wt%, a significant nanoparticle aggregation was observed on the membrane surface (Fig. 3f). It should be noted that for conventional mixed matrix and nanocomposite membranes, the loading of the MOF filler is limited due to the difficulty in maintaining a uniform and even distribution within the polymeric matrix. The MOF aggregation can potentially lead to non-selective defects and particle loss during the fabrication process. As a result, most previous work has only studied a relatively low particle loading (<30 wt%).^{25,30} In this work, up to

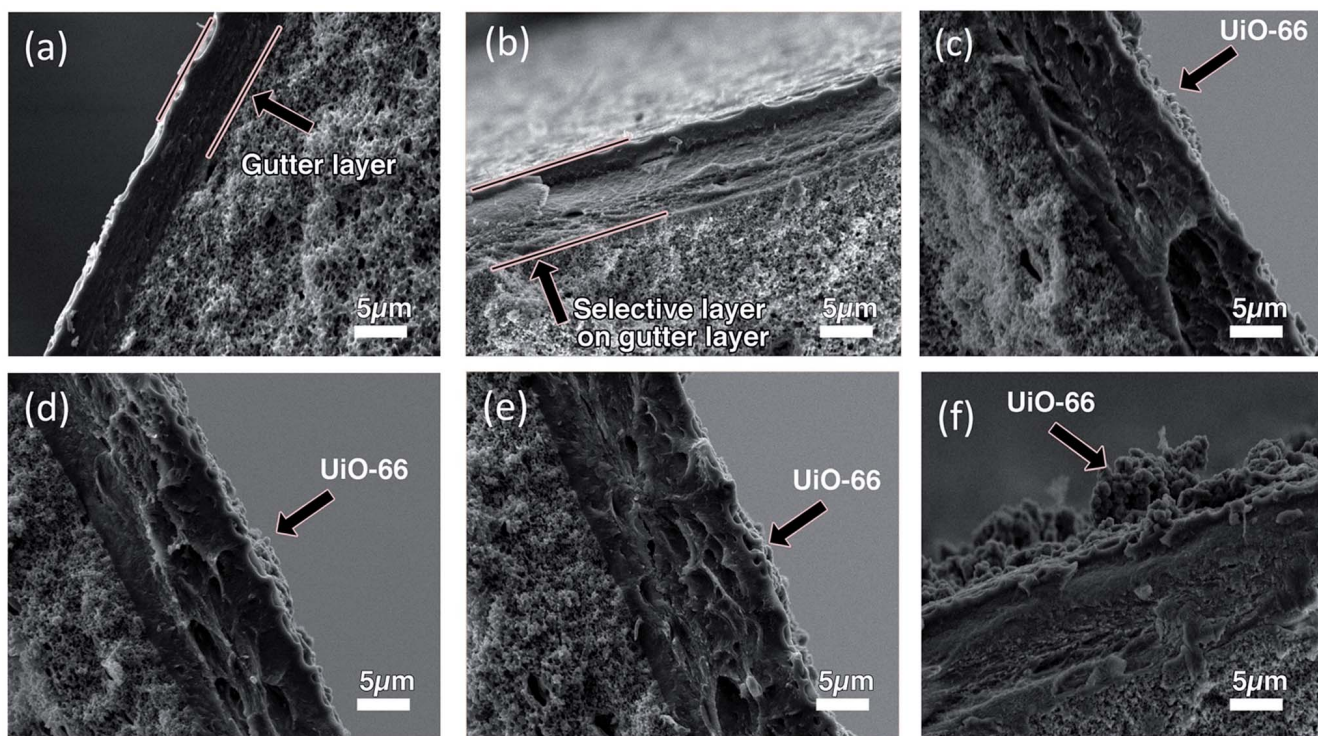


Fig. 3 Cross-sectional SEM images of composite membranes with different coating layers: (a) PTMSP, (b) PTMSP and pure Pebax, (c) PTMSP and 50 wt% UiO-66 in Pebax, (d) PTMSP and 50 wt% UiO-66-NH₂ in Pebax, (e) PTMSP and 50 wt% UiO-66-(COOH)₂ in Pebax and (f) PTMSP and 80 wt% UiO-66 in Pebax. Membranes (b–f) have an extra top Pebax protective layer.

80 wt% of MOFs were blended into the Pebax dip-coating solution. At low to moderate UiO-66 loadings (10–50 wt%), the particles were evenly distributed without significant aggregation, and clear UiO-66 aggregation was only observed at 80 wt% MOF loading (Fig. S3[†] and 3). In addition, it should be noted that compared with the composite membrane with a pure Pebax layer, the composite membrane containing 80 wt% of UiO-66 had comparable tensile strength (elongation at break: 35% and 37% and tensile strength at break: 3.1 and 2.9 MPa, respectively), indicating a good compatibility between the MOF and Pebax.

To confirm the presence of UiO-66 particles (or those of its derivatives) inside the composite membranes, EDX scanning of Zr was conducted. Typical results for UiO-66 are presented in Fig. 4. The Zr content of UiO-66 particles can be observed near the top surface of the composite membrane with a thickness of around 1–1.5 μm for all samples. This confirms the observation from SEM that the thickness beyond the PTMSP gutter layer was around 1–1.5 μm. The Zr signal strength within the selective layer increased with a higher particle loading (from 10 wt% to 80 wt%). The EDX scan can provide a rough indication of the selective layer thickness. However, it must be noted that the exact thickness of the selective layer and the top protective layer was difficult to measure due to the interfusion of the PTMSP and Pebax layers during the repeated coating process. In addition, for a membrane with high UiO-66 loading (80 wt%), it is difficult to accurately determine its selective layer thickness due to the nanofiller aggregation. Based on the SEM image (Fig. 3),

the UiO-66 aggregates can be up to 10 μm on the membrane surface.

3.2.2 The crystallinity of the composite membrane. XRD analysis was performed to determine the crystal structure of the membranes. Four common crystal phases (α , β , γ , and δ) have been reported for PVDF.⁵¹ The crystallinity of PVDF is one of the most important factors influencing its mechanical properties. The XRD patterns of the composite membranes are shown in

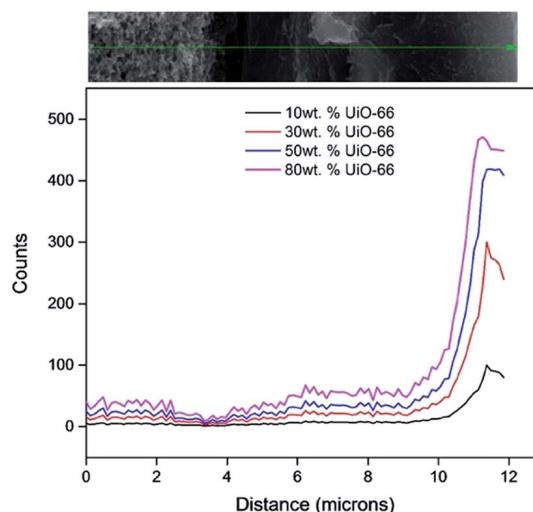


Fig. 4 EDX linear scanning of the Zr content of the cross section of membranes containing different UiO-66 loadings.

Fig. S4,[†] and the observed characteristic peak at $\theta = 20.17^\circ$ for all membranes originated from the PVDF supporting membrane (β phase).⁵ After the membrane coating with a PTMSP gutter layer, a broad signature peak of the PTMSP polymer at 10° was observed. The signature peak of Pebax-1657 at 24.1° for the crystalline polyamide phase and the broader peak of the polyethylene oxide phase from 17.5° to 22.5° could not be observed clearly from the XRD patterns of the composite membranes.²⁵ This can be mainly attributed to a thin Pebax layer as well as their overlap with the peaks of PVDF. To better highlight the preservation of UiO-66 crystallinity within Pebax, we conducted XRD analysis with UiO-66/Pebax-1657 mixed matrix films (Fig. 5). It shows that after the addition of UiO-66 nanoparticles, the signature peaks of UiO-66 (Fig. S2[†]) were clearly observed, indicating the preservation of crystallinity of particles inside the layer for the mixed matrix films.

DSC analysis was also carried out to study the evolution of the melting point (T_m) of the composite membrane (Table 2). The pure PVDF membrane had a T_m of around 157°C and after the coating of PTMSP and Pebax layers, the T_m value increased to a slightly higher value. After incorporation of the UiO-66, the melting point further increased to around 165°C , indicating a good interfacial compatibility between UiO-66 and its surrounding Pebax matrix, which could rigidify the polymer chains.

It is important to explore the effect of UiO-66 on the polymeric structure of the Pebax selective layer. However, it can be challenging to characterize the thin selective layer within the composite membrane. Therefore, we fabricated a series of thick mixed matrix membranes with UiO-66 and Pebax. The degree of crystallinity in both soft and hard phases of Pebax was analysed using DSC and estimated using eqn (5):

$$X_c = \frac{\Delta H_m}{\Delta H_m^0} \quad (5)$$

where ΔH_m is the tested melting enthalpy of a certain polymeric section and ΔH_m^0 is the melting enthalpy of its fully crystalline

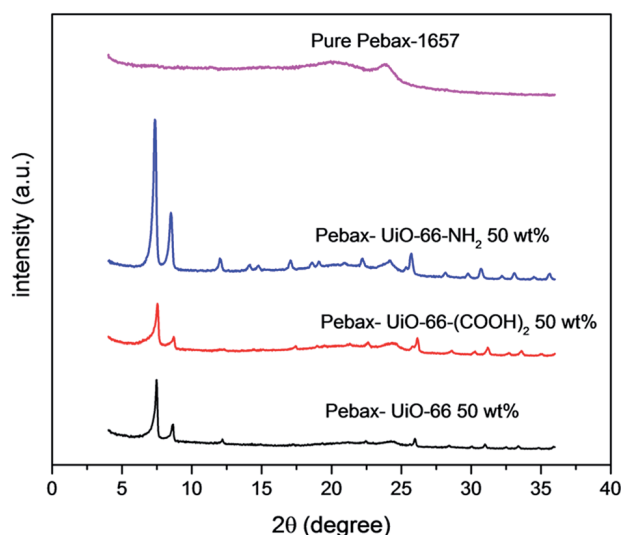


Fig. 5 XRD patterns of the different UiO-66/Pebax-1657 mixed matrix membranes.

Table 2 Melting point (T_m) of the UiO-66/Pebax-1657-based composite membranes (typical error of T_m was around 0.5°C)

Type of membrane	T_m ($^\circ\text{C}$)
Pure PVDF	157
PTMSP coated	159
PTMSP + Pebax coated	160
50 wt% UiO-66/Pebax coated	164
50 wt% UiO-66-NH ₂ /Pebax coated	165
50 wt% UiO-66-(COOH) ₂ /Pebax coated	164

form. The melting enthalpy (ΔH_m) was estimated from the area of the melting peak in the DSC curves, while the melting enthalpy of the pure crystalline phase (ΔH_m^0) of PEO is 166.4 J g^{-1} and PA is 230 J g^{-1} .⁵² The degrees of crystallinity of the PA and PEO phases of pure Pebax and UiO-66/Pebax are presented in Table 3. After the incorporation of UiO-66, especially the functionalized UiO-66 nanoparticles, both PA and PEO phases showed enhancements in crystallinity. This indicates an increase in the rigidity of the polymer matrix after the incorporation of particles due to the potential formation of hydrogen bonds between polymeric chains and UiO-66.

3.2.3 Chemical properties of the UiO-66/Pebax-1657 composite membranes. To examine the chemical structure of pure PVDF and the composite membranes, FTIR analysis was conducted. The FTIR spectra of pure PVDF and typical composite membranes incorporating 50 wt% UiO-66 are depicted in Fig. 6. The peak for pure PVDF at 1403 cm^{-1} was attributed to CH_2 vibrations, and the C-C band of PVDF was observed at 1185 cm^{-1} . The CF_2 stretching vibration and bending modes were observed as peaks at around $745\text{--}840$ and 510 cm^{-1} , respectively. The bands located at around 3022 and 2980 cm^{-1} corresponded to the CH_2 asymmetric and symmetric vibration of PVDF.⁵¹ After deposition of the Pebax-1657 mixture, the stretching vibration of the C-O-C group in the PEO segment of Pebax appeared as a distinct peak at around 1094 cm^{-1} . In addition, the PA segment in Pebax exhibited additional peaks at 3297 cm^{-1} for N-H , 1636 cm^{-1} for H-N-C=O and 1730 cm^{-1} for O-C=O groups.^{52,53} Previous research studies have demonstrated that MOFs can form hydrogen bonds with the glassy section of Pebax.^{25,30} But the N-H peak shift for the PA segment is negligible in this work (Fig. 6b), possibly due to the difficulty in characterizing the thin composite layer.

3.3 The gas separation performance of various UiO-66-based membranes

In the case of mixed matrix membranes, it is relatively difficult to incorporate a large percentage of nanofillers into the matrix due to the difficulty in obtaining a homogeneous dispersion, as well as the loss in mechanical strength. In the present work, we incorporated up to 80 wt% of UiO-66 into the thin Pebax layer and the gas separation performance was investigated with both pure gases and mixed gases. Both PDMS and PTMSP were applied as gutter layers and the results are summarized in Table S1.[†] PTMSP clearly had higher CO_2 permeance and selectivity.

Table 3 The degree of crystallinity of PA and PEO phases in Pebax-based dense mixed matrix membranes

Type of membrane	Integral of melting peak (J g^{-1})			X_{PEO} (%)	X_{PA} (%)	X_{c} (total) (%)
	PEO block	PA block				
Pure Pebax	14.72	21.1		14.74	22.93	18.02
50 wt% UiO-66/Pebax	18.10	22.43		18.13	24.38	20.63
50 wt% UiO-66-(COOH) ₂ /Pebax	19.46	23.06		19.49	25.07	21.72
50 wt% UiO-66-NH ₂ /Pebax	19.89	23.19		19.92	25.22	22.04

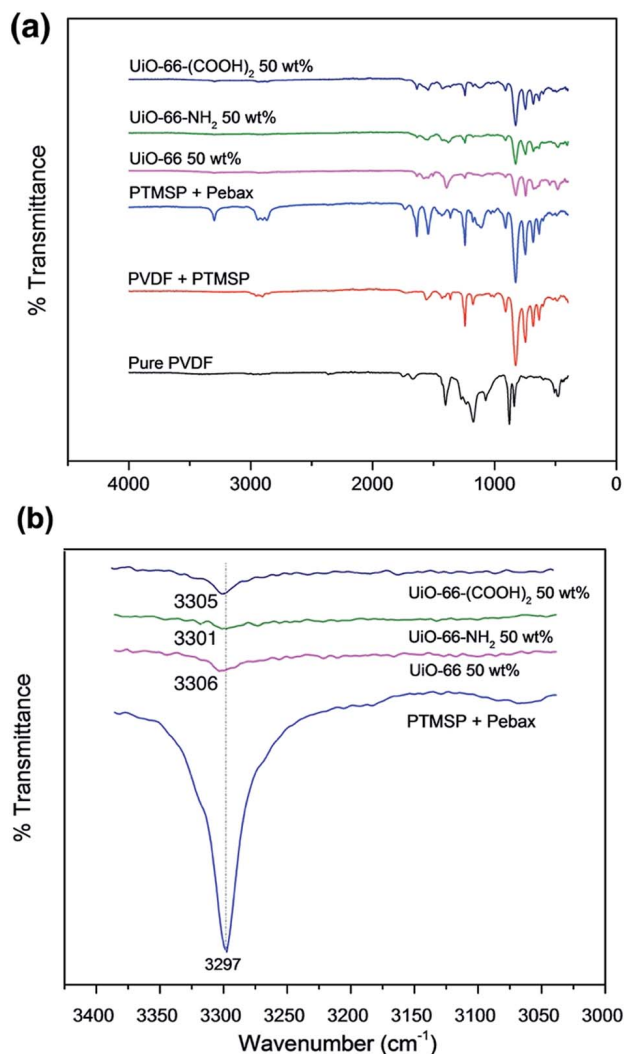


Fig. 6 (a) FTIR spectra of the different UiO-66/Pebax-1657 nano-composite membranes and (b) the enlarged wavenumber range between 3000 and 3400 cm^{-1} .

As a result, PTMSP was applied for membrane fabrication in the subsequent tests. A smooth gutter layer can prevent the intrusion of Pebax into supportive membrane pores, ensuring a thin and continuous selective layer. Fig. 7 presents the gas permeation performance of UiO-66/Pebax-1657-based composite membranes with various particle loadings. In terms of the composite membrane containing pure Pebax as the selective layer, the CO_2 permeability was much higher than that of other

gases such as N_2 and CH_4 , which could be attributed to the rubbery PEO block in Pebax which has a strong affinity to polar gas (CO_2) over non-polar gases (N_2 and CH_4).^{54,55}

Compared with the pure Pebax membrane, the incorporation of UiO-66 into the selective layer only slightly increased the CO_2 permeance, even for the membrane containing 80 wt% of UiO-66. These results are unexpected considering the large BET surface area of UiO-66 and its relatively wide BJH pore diameter range compared with the target CO_2 molecules (Table 1). Within the thin composite selective layer, the gas transport can be affected by the polymeric sections, MOF structures and MOF-polymer interfacial regions.^{25,33,55} The relatively unchanged CO_2 permeance indicates a good interfacial compatibility; otherwise rapid gas transport can occur *via* the non-selective defect voids throughout the thin layer. As suggested in Table 3, the addition of UiO-66 into Pebax can effectively increase the crystallinity and thereby rigidify the polymer chains, which slows the gas transport. As a result, the CO_2 permeance only slightly increased with the addition of UiO-66, even though its inherent highly porous structure can facilitate rapid gas molecule transport. In terms of the gas selectivity (Fig. 7b and c), for the membrane with UiO-66, the highest selectivity was observed with a nanofiller loading of 50 wt% for both CO_2/N_2 and CO_2/CH_4 . It should be noted that the increased selectivity should mainly originate from the increased polymer chain rigidity as the pore size of UiO-66 (Table 1) is unlikely to provide effective molecular sieving for CO_2 against N_2 and CH_4 .

The functionalization of UiO-66 can have a significant effect on the composite membrane performance. Compared with UiO-66, much higher CO_2 permeance results were obtained for all membranes with different UiO-66-NH₂ nanofiller loadings. Based on our previous gas adsorption results, the presence of amine groups on the organic ligands appear to have improved the selective CO_2 uptake for UiO-66-NH₂, leading to higher CO_2 solubility within the thin selective layer.

On the other hand, for the UiO-66-(COOH)₂ nanofillers, the MOF pore blockage by the carboxylate functional groups limited its gas adsorption within the framework structure, such that its incorporation into the Pebax matrix had a relatively minor effect on CO_2 permeance, similar to the case of the UiO-66. For both functionalized MOFs, the highest selectivities were obtained at 50 wt% loading, suggesting good compatibility between nanofillers and the polymeric matrix. Based on the gas permeation results with the functionalized UiO-66, we can further confirm that the composite membrane performance is dominated by the interactions between nanofillers and the polymer matrix: the

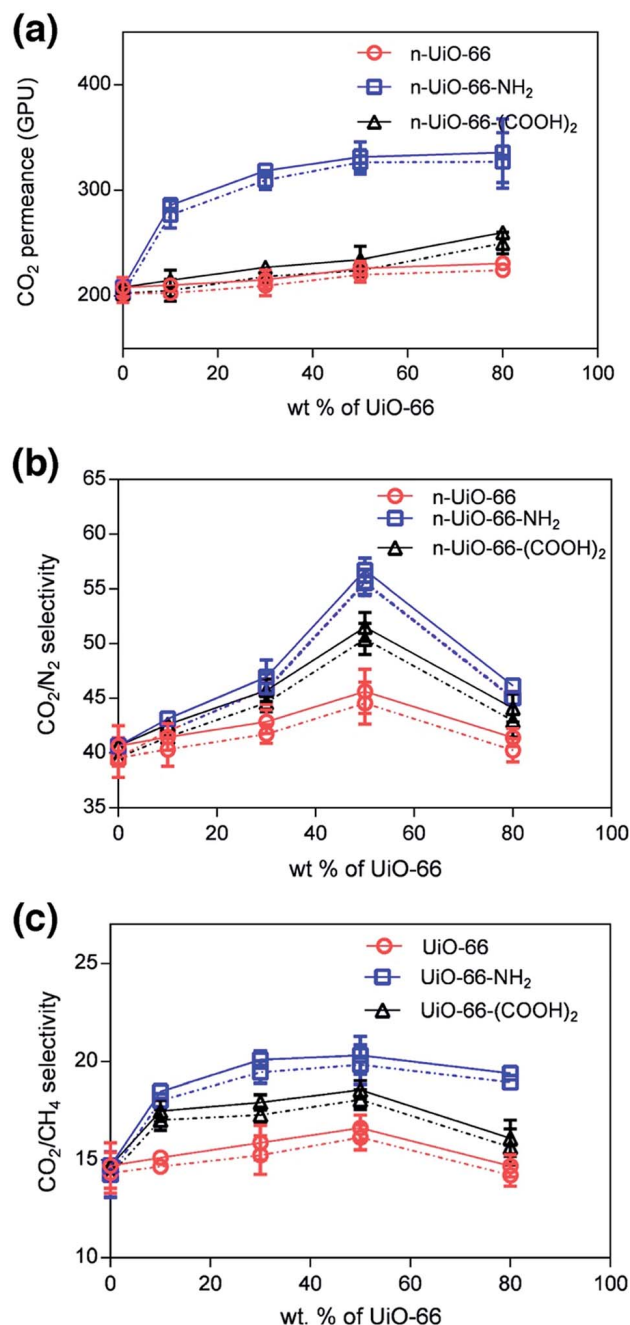


Fig. 7 Gas separation performance of UiO-66/Pebax-1657-based composite membranes at different particle loadings: (a) CO₂ permeance, (b) CO₂/N₂ gas selectivity and (c) CO₂/CH₄ gas selectivity (solid lines represent pure gas and dashed lines represent mixed gas).

highest gas permeance and selectivity were obtained with UiO-66-NH₂, the BET surface area of which was significantly lower than that of UiO-66. In addition, even though the COOH functionalized UiO-66 had the smallest BJH pore size, the functionalized MOF pore was still too large for effective molecular sieving; therefore the shrinkage in pore size did not effectively lead to an improved selectivity.⁵⁶ In this work, we also conducted the Maxwell model calculation for the composite membranes. However, the model failed to accurately predict the composite membrane performance, possibly because the effect

of interfacial region was not considered by the Maxwell model. A more detailed discussion and Maxwell model results are presented in the ESI (Fig. S5).†

3.4 The effects of operating pressure and plasticization on gas separation performance

Membrane plasticization caused by polymer chain swelling is a common phenomenon for gas separation membranes when exposed to aggressive feed conditions,^{57,58} e.g., CO₂ separation from CH₄ in natural gas treatment. The condensable gas increases the mobility of the polymer chain segments, which further increases the diffusion coefficients of all penetrants through the polymer membrane. This eventually leads to the increase of permeability and loss of selectivity. For a polymer membrane, the plasticization pressure is defined as the pressure at which the gas permeability increases with increasing feed pressure.⁵⁹

Pebax has been thoroughly investigated as a promising candidate for industrial CO₂ separation.^{17,37,60} However, the behavior of the Pebax-based mixed matrix membrane under elevated operating pressures has not been fully elucidated, especially for the thin Pebax layer within a composite hollow fiber membrane. In this study, we exposed the UiO-66/Pebax composite membrane to different feed pressures in a complete pressurization–depressurization cycle to investigate the reversibility of the polymer matrix swelling/compaction effect. In order to understand the effect of membrane plasticization on the non-condensable gas permeation, CH₄ permeation tests were also carried out upon completion of the CO₂ permeation experiment under each tested pressure.⁶¹ The best-performing membranes (containing 50 wt% of UiO-66 and its derivatives) were tested here.

The gas permeation results for the UiO-66/Pebax-based composite membranes are presented in Fig. 8 and S6.† The experiment was carried out at up to 15 bar, as further increasing the feed pressure can lead to the collapse of the supporting membranes. In general, the membranes showed a decrease in CO₂ permeability with the increase of feed pressure. Previous studies have revealed that gas transport through pure Pebax-based membranes occurs mostly through the soft PEO block.^{54,55} Therefore, the effect of pressure on the gas permeability was based on the competing effects of hydrostatic pressure and plasticization.^{25,55} CO₂ gas permeance through the pure Pebax-coated membrane at elevated pressure showed a relatively severe decrease, to almost half of its initial value at 2 bar, due to a compaction effect of the polymer matrix. The gas permeance did not return to its initial value during the depressurization process indicating that the polymer matrix was irreversibly compacted. In addition, up to 15 bar, the membranes did not show an obvious plasticization effect as observed in the glassy polymer.

The incorporation of UiO-66 and its derivatives helped to reduce the compaction effect as can be seen from the relatively stable gas permeance at different feed pressures. Our previous study on ZIF-8/Pebax-1657-based composite membranes showed a similar phenomenon.²⁵ The increase in the rigidity of

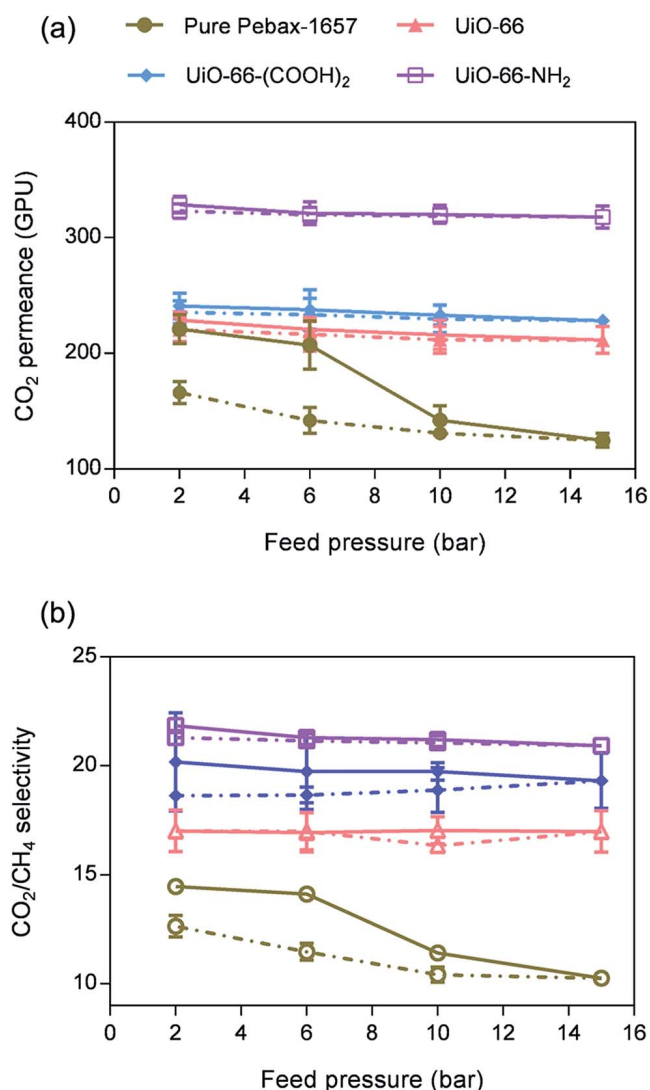


Fig. 8 The effect of feed pressure on (a) CO₂ permeance, and (b) CO₂/CH₄ selectivity of various UiO-66/Pebax-1657-based composite membranes (solid lines represent the pressurization step and dashed lines represent the depressurization step).

the polymer matrix helped to increase the compaction resistance of the membranes incorporating UiO-66 particles. The increase in the rigidity of the membranes was reflected in the increase in melting point and the degree of crystallinity as shown in Tables 2 and 3. All the membranes incorporating particles showed good compaction resistance during the experiment.

CH₄ gas permeation tests were also conducted directly after the CO₂ permeation test at each pressure to analyse the plasticization/compaction effect on the permeation of the non-condensable gas. The results of the CH₄ permeance and CO₂/CH₄ gas selectivity are presented in Fig. 8b and S6.† Compaction of the polymer matrix at elevated pressures also affected the CH₄ gas permeance through the membranes, leading to lower permeance for the pure Pebax coated membranes. Again, the incorporation of UiO-66 particles helped to improve the compaction resistance of the membranes. In terms of gas

selectivity, a relatively constant CO₂/CH₄ selectivity was observed in membranes incorporating UiO-66 particles. On the other hand, a decrease in gas selectivity with the increase of feed pressure was observed in the pure Pebax membrane, as this membrane experienced a relatively severe compaction effect.

3.5 ZIF-7/Pebax-1657-based hollow fiber composite membranes

Based on our results on the utilization of UiO-66 and its derivatives for composite membrane fabrication, it is very important to investigate the effect of surface functional groups and pore size on the final membrane performance, especially at elevated pressures. In addition, to understand the general applicability of the membrane fabrication method used in this work, we also fabricated ZIF-7/Pebax-1657-based composite membranes using a similar dip coating approach to that used for the UiO-66/Pebax-based membranes. ZIF-7 has a window aperture of ~3.0 angstroms, which is smaller than the kinetic diameter of CO₂ gas (~3.4 angstroms). However, previous studies on ZIF-7 revealed the flexible nature of ZIF-7's apertures^{37,62} that provided an enhancement in CO₂ uptake by the framework at a relatively high pressure, which is in good agreement with the results obtained in this work (Fig. 3).

3.5.1 Gas separation performance of the ZIF-7/Pebax-based hollow fiber composite membranes. In this experiment, ZIF-7/Pebax-1657-based membranes with 10–30 wt% particle loading were synthesized and tested for their gas separation performance. Further increasing the ZIF-7 content in the coating solution would lead to particle aggregation and settling. The SEM images of the composite membrane are presented in Fig. S7:† at 30 wt% of ZIF-7 loading, clear nanoparticle aggregation can be observed. We further tested the membrane performance with both pure and mixed gases (Fig. 9). Both pure gas and mixed gas showed similar results, with only marginally lower gas permeance for the mixed gas due to a competitive sorption effect. The incorporation of ZIF-7 slightly increased the CO₂ permeance through the membranes, which can be attributed to the small pore size of ZIF-7.

Our previous study on ZIF-8/Pebax-1657-based membranes suggests the loss of gas selectivity of the nanocomposite membranes.²⁵ The incorporation of MOF particles with flexible framework structures could allow the rapid transport of bulkier gas molecules. It could also create microvoids in the interfacial region. In comparison, the incorporation of ZIF-7 slightly increased the gas selectivity. A similar increase in gas selectivity with higher particle loading was also reported in a previous study on flat sheet membranes containing ZIF-7.³⁷

3.5.2 Gas separation performance of the ZIF-7/Pebax-1657-based hollow fiber composite membranes at elevated pressure. The effects of elevated pressure on CO₂ and CH₄ gas permeances are depicted in Fig. 10 and S8.† The competing effects of compaction and plasticization resulted in a decrease of gas permeance for all the membranes tested. Compared to the pure Pebax membrane, the decreases in gas permeance in the ZIF-7/Pebax-1657-based membranes were less severe. This

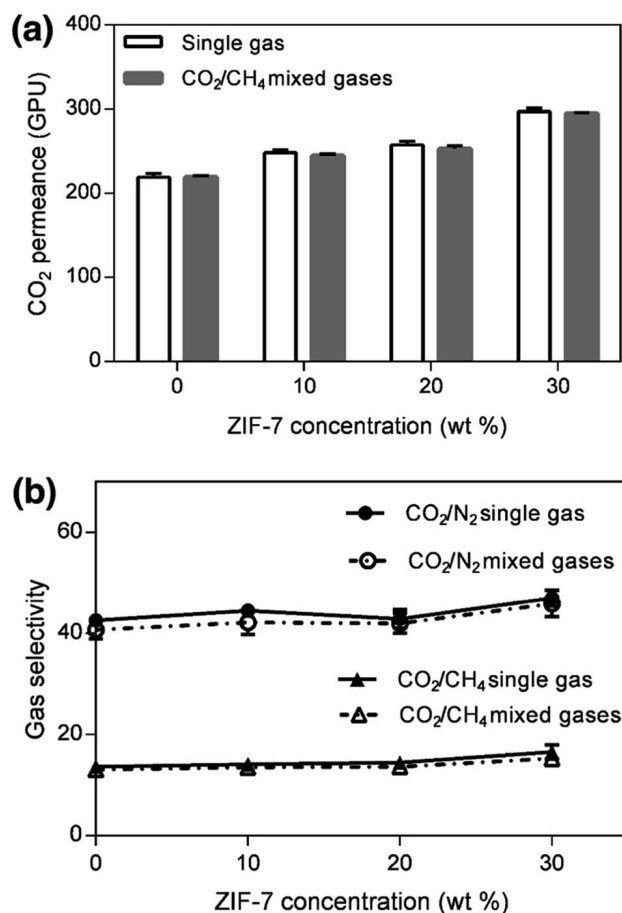


Fig. 9 Gas separation performance of ZIF-7/Pebax-1657-based composite membranes at different particle loadings: (a) CO₂ permeance, (b) CO₂/N₂ and CO₂/CH₄ gas selectivity (solid lines represent pure gas and dashed lines represent mixed gas).

shows an increase in polymer rigidity after the incorporation of the particles, as was observed for the UiO-66/Pebax-1657-based membranes (Section 3.4).

3.6 Comparison of gas separation performance and understanding the effect of MOF rigidity

Recently, there have been a number of studies on nano-composite membranes incorporating MOFs. To better understand how the MOF functions within the thin selective layer, the results obtained in this work are compared with our previous results using ZIF-8 nanocrystals in addition to other relevant reports (Table 4). In the present work, the incorporation of UiO-66 and ZIF-7 into the composite membranes increased both CO₂ permeance and gas selectivity. The highest CO₂/N₂ selectivity obtained with 50 wt% UiO-66 was 57 with a CO₂ permeance of 338 GPU, making this membrane one of the best performing MOF-containing composite membranes (Table 4). It should be noted that by optimizing the dip-coating substrates, gutter layer materials, coating technique and coating material solution, some pure polymer composite membranes can exhibit comparable gas separation performance.^{21,67,68} However, as suggested earlier, the operational

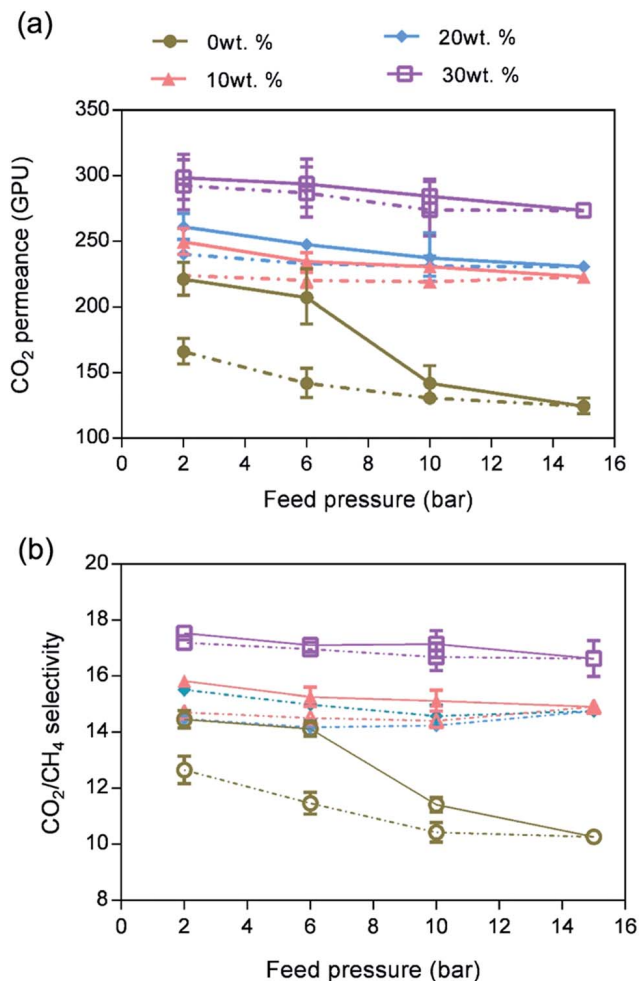


Fig. 10 (a) CO₂ gas permeances and (b) CO₂/CH₄ selectivity at different feed pressures of ZIF-7/Pebax-1657-based composite membranes (solid lines represent the pressurization step and dashed lines represent the depressurization step).

stability of the pure polymer membrane still limits its industrial application under harsh conditions.

In our previous work, the addition of ZIF-8 into the thin Pebax layer led to the loss of its gas selectivity.²⁵ In comparison, both improved gas permeance and selectivity were obtained with UiO-66 and ZIF-7 in this work. The addition of ZIF-8 into the Pebax polymeric layer may rigidify the polymeric chains *via* hydrogen bonding, and their crystalline framework structure may ensure high molecular sieving capabilities. Both of these aspects can improve the gas selectivity of the composite membranes. On the other hand, it has been demonstrated that the organic ligand of ZIF-8 can experience pore-gate-opening due to the rotational and vibrational movement of the organic ligands, which can be attributed to the bending of the N-Zn-N bond and rotation of the Zn-MeIM-Zn bond of ZIF-8.²⁷ This can reduce the intrinsic molecular separation capability of the ZIF-8. At the same time, since ZIF-8 is considered as a “flexible” MOF due to its low metal-center-coordination number, it may experience conformational changes under external mechanical

Table 4 Comparison of the performance of nanocomposite membranes incorporating different particles in CO₂/N₂ gas separation

Support	Gutter layer	Selective layer	Membrane type	Max. particle loading	Testing T/P (°C/bar)	CO ₂ permeance (GPU)	CO ₂ /N ₂ selectivity	Ref.
PAN	PDMS	Pebax-2533/soft PEG- <i>b</i> -PDMS nanoparticle	Flat sheet	40 wt%	35/3.4	1374	12	63
PAN	PDMS	Pebax-2533/soft PEG-based nanoparticle	Flat sheet	50 wt%	35/3.4	601	28	64
PAN	PDMS	Pebax-2533/PRXs soft nanoparticle	Flat sheet	30 wt%	35/3.4	1670	14	65
PAN	PTMSP	Pebax-1657/ZIF-7	Flat sheet	34 wt%	20/3.75	39	105	37
PVDF	—	Pebax-1657/UiO-66	Flat sheet	20 wt%	25/3	~130 barrer	20	30
PVDF	—	Pebax-1657/UiO-66-NH ₂	Flat sheet	20 wt%	25/3	~125 barrer	25	30
PSf	—	PDMS/Cu ₃ (BTC) ₂	Hollow fiber	4000 ppm	25/5	109.2	33.46	66
PVDF	PTMSP	Pebax-1657/ZIF-8	Hollow fiber	30 wt%	25/2	345	31.7	25
PVDF	PTMSP	Pebax-1657/UiO-66	Hollow fiber	50 wt%	25/2	225	45	This work
PVDF	PTMSP	Pebax-1657/UiO-66-NH ₂	Hollow fiber	50 wt%	25/2	338	57	work
PVDF	PTMSP	Pebax-1657/UiO-66-(COOH) ₂	Hollow fiber	50 wt%	25/2	240	50	
PVDF	PTMSP	Pebax-1657/ZIF-7	Hollow fiber	30 wt%	25/2	300	48	

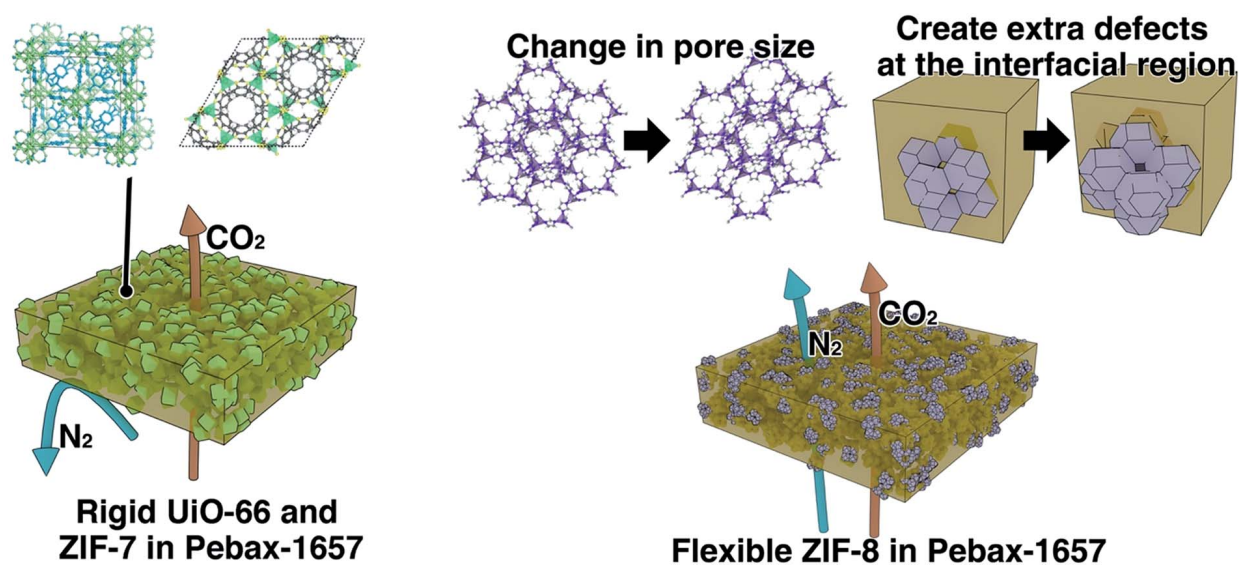


Fig. 11 Schematic diagram of the UiO-66, ZIF-7 and ZIF-8 nanocomposite membranes.

stress. All these aspects may eventually lead to the loss of selectivity.

On the other hand, both UiO-66 and ZIF-7 are considered more rigid. For example, UiO-66 has an ultrahigh shear modulus of ~14 GPa (compared with ~1 GPa for flexible ZIF-8).³¹ The high Zr–O coordination restricts the bending of the bonds, which can effectively preserve its intrinsic molecular sieving capability within a polymeric matrix (Fig. 11). As a result, the incorporation of rigid UiO-66 can simultaneously improve gas permeance and selectivity of the composite membranes. This may also explain why the incorporation of ZIF-7 showed an improved membrane gas selectivity: ZIF-7 and ZIF-8 have similar crystalline structures, but ZIF-7 has a more rigid framework structure.²⁶ Still, in order to fully understand the effect of MOF rigidity on the membrane performance, more characterization should be carried out to investigate the MOF structure within the polymeric matrix. However, this is beyond the scope of this work.

4 Conclusions

In this work, UiO-66 and ZIF-7/Pebax based hollow fiber composite membranes were fabricated. Functionalized UiO-66 was applied to understand the effect of surface modification on the final membrane performance. The addition of nanofillers can effectively promote the gas permeance. Due to good interfacial compatibility, the Pebax thin layer can host 50 wt% UiO-66 without introducing extra defects and further increase the UiO-66 loading to 80 wt% with only slightly reduced gas selectivity. This work also investigated the operational stability of the nanocomposite membranes, and the results indicate that the addition of nanofillers can rigidify the Pebax polymer chains *via* hydrogen bonds, which subsequently enhances the plasticization and compaction resistance of both UiO-66 and ZIF-7 composite membranes. Finally, we discussed the effect of MOF rigidity on the final membrane performance and suggested that more rigid MOFs

are preferred to maintain their intrinsic molecular sieving capability within the thin composite membranes.

Conflicts of interest

There are no conflicts to declare.

Acknowledgements

This work was supported by the Science and Industry Endowment Fund (SIEF Grant ID RP02-035, CO2MOF) project. Putu Doddy Sutrisna would like to acknowledge support from Australia Awards Scholarship (AAS) and Australia Leadership Awards Scholarship (ALAS) for scholarships provided. The authors would like to acknowledge Dr Peter Southon of the School of Chemistry, University of Sydney and Dr Jason Scott of the School of Chemical Engineering, UNSW for their help and discussions in conducting BET and gas sorption experiments.

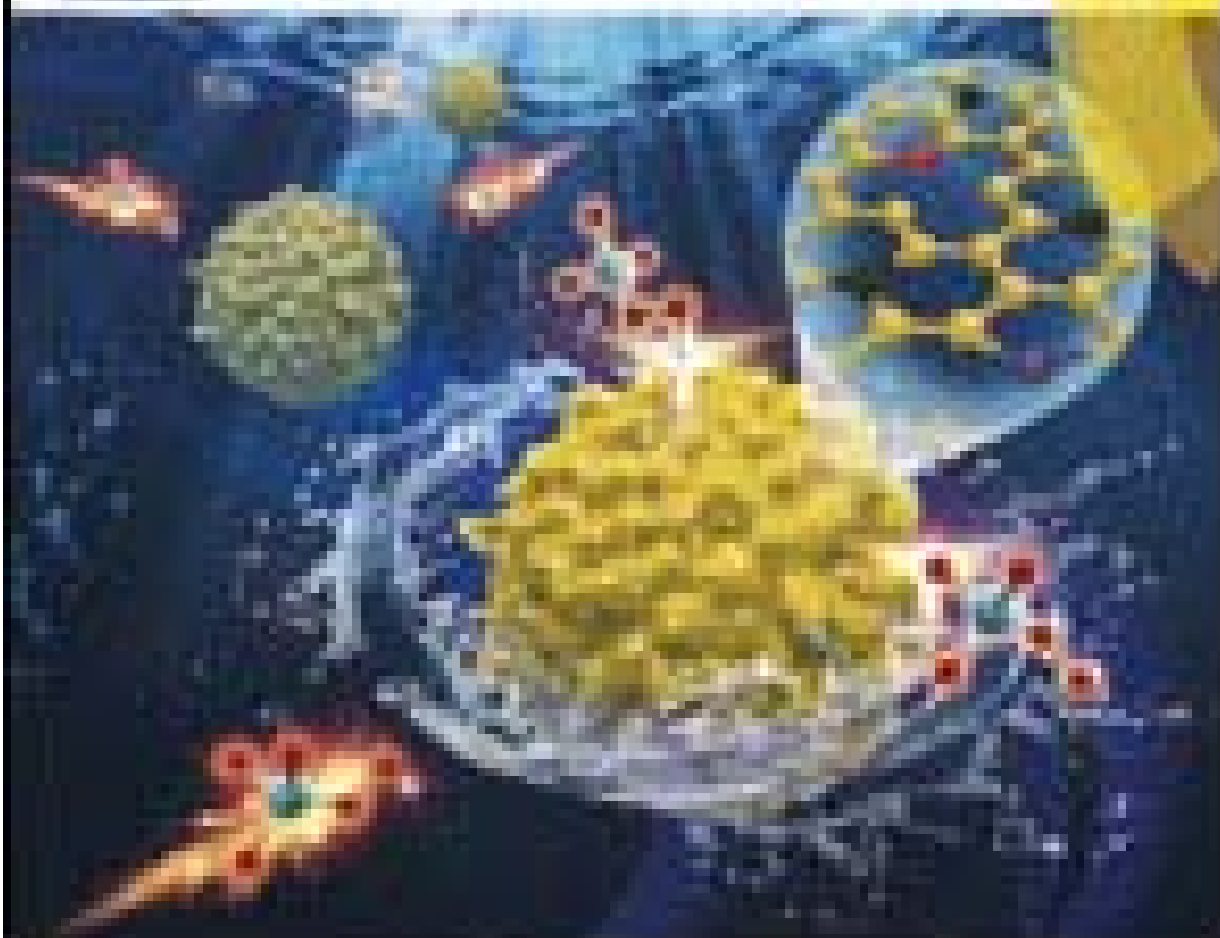
Notes and references

- W. J. Koros and G. K. Fleming, *J. Membr. Sci.*, 1993, **83**, 1–80.
- P. Bernardo, E. Drioli and G. Golemme, *Ind. Eng. Chem. Res.*, 2009, **48**, 4638–4663.
- S. Zhao, P. H. M. Feron, L. Deng, E. Favre, E. Chabanon, S. Yan, J. Hou, V. Chen and H. Qi, *J. Membr. Sci.*, 2016, **511**, 180–206.
- D. M. D'Alessandro, B. Smit and J. R. Long, *Angew. Chem., Int. Ed.*, 2010, **49**, 6058–6082.
- J. Hou, P. D. Sutrisna, Y. Zhang and V. Chen, *Angew. Chem.*, 2016, **128**, 4015–4019.
- J.-R. Li, R. J. Kuppler and H.-C. Zhou, *Chem. Soc. Rev.*, 2009, **38**, 1477–1504.
- Y. Zhang, H. Wang, J. Liu, J. Hou and Y. Zhang, *J. Mater. Chem. A*, 2017, **5**, 19954–19962.
- H. B. Tanh Jeazet, S. Sorribas, J. M. Román-Marín, B. Zornoza, C. Téllez, J. Coronas and C. Janiak, *Eur. J. Inorg. Chem.*, 2016, **2016**, 4363–4367.
- E. M. Mahdi and J.-C. Tan, *J. Membr. Sci.*, 2016, **498**, 276–290.
- T.-S. Chung, L. Y. Jiang, Y. Li and S. Kulprathipanja, *Prog. Polym. Sci.*, 2007, **32**, 483–507.
- B. Zornoza, C. Tellez, J. Coronas, J. Gascon and F. Kapteijn, *Microporous Mesoporous Mater.*, 2013, **166**, 67–78.
- G. Dong, H. Li and V. Chen, *J. Mater. Chem. A*, 2013, **1**, 4610–4630.
- L. M. Robeson, *J. Membr. Sci.*, 2008, **320**, 390–400.
- R. Lin, L. Ge, L. Hou, E. Strounina, V. Rudolph and Z. Zhu, *ACS Appl. Mater. Interfaces*, 2014, **6**, 5609–5618.
- Z. Wang, D. Wang, S. Zhang, L. Hu and J. Jin, *Adv. Mater.*, 2016, **28**, 3399–3405.
- C. Zhang, Y. Dai, J. R. Johnson, O. Karvan and W. J. Koros, *J. Membr. Sci.*, 2012, **389**, 34–42.
- V. Nafisi and M.-B. Hägg, *J. Membr. Sci.*, 2014, **459**, 244–255.
- S. Shahid and K. Nijmeijer, *J. Membr. Sci.*, 2014, **470**, 166–177.
- S. Shahid and K. Nijmeijer, *J. Membr. Sci.*, 2014, **459**, 33–44.
- B. A. Al-Maythaly, A. M. Alloush, M. Faizan, H. Dafallah, M. A. A. Elgzoly, A. A. A. Seliman, A. Al-Ahmed, Z. H. Yamani, M. A. M. Habib, K. E. Cordova and O. M. Yaghi, *ACS Appl. Mater. Interfaces*, 2017, **9**, 33401–33407.
- H. Z. Chen, Z. Thong, P. Li and T.-S. Chung, *Int. J. Hydrogen Energy*, 2014, **39**, 5043–5053.
- M. Benzaqui, R. Semino, N. Menguy, F. Carn, T. Kundu, J.-M. Guigner, N. B. McKeown, K. J. Msayib, M. Carta, R. Malpass-Evans, C. Le Guillouzer, G. Clet, N. A. Ramsahye, C. Serre, G. Maurin and N. Steunou, *ACS Appl. Mater. Interfaces*, 2016, **8**, 27311–27321.
- K. Eum, C. Ma, A. Rownaghi, C. W. Jones and S. Nair, *ACS Appl. Mater. Interfaces*, 2016, **8**, 25337–25342.
- P. Neelakanda, E. Barankova and K.-V. Peinemann, *Microporous Mesoporous Mater.*, 2016, **220**, 215–219.
- P. D. Sutrisna, J. Hou, H. Li, Y. Zhang and V. Chen, *J. Membr. Sci.*, 2017, **524**, 266–279.
- J. C. Tan and A. K. Cheetham, *Chem. Soc. Rev.*, 2011, **40**, 1059–1080.
- M. R. Ryder, B. Civalleri, T. D. Bennett, S. Henke, S. Rudić, G. Cinque, F. Fernandez-Alonso and J.-C. Tan, *Phys. Rev. Lett.*, 2014, **113**, 215502.
- J.-C. Tan, B. Civalleri, C.-C. Lin, L. Valenzano, R. Galvelis, P.-F. Chen, T. D. Bennett, C. Mellot-Draznieks, C. M. Zicovich-Wilson and A. K. Cheetham, *Phys. Rev. Lett.*, 2012, **108**, 095502.
- C. Zhang, R. P. Lively, K. Zhang, J. R. Johnson, O. Karvan and W. J. Koros, *J. Phys. Chem. Lett.*, 2012, **3**, 2130–2134.
- J. Shen, G. Liu, K. Huang, Q. Li, K. Guan, Y. Li and W. Jin, *J. Membr. Sci.*, 2016, **513**, 155–165.
- H. Wu, T. Yildirim and W. Zhou, *J. Phys. Chem. Lett.*, 2013, **4**, 925–930.
- W. Liang, R. Babarao, M. J. Murphy and D. M. D'Alessandro, *Dalton Trans.*, 2014, **44**, 1516–1519.
- X. Liu, N. K. Demir, Z. Wu and K. Li, *J. Am. Chem. Soc.*, 2015, **137**, 6999–7002.
- X. Liu, C. Wang, B. Wang and K. Li, *Adv. Funct. Mater.*, 2017, **27**, 1604311.
- C. Wang, M. Lee, X. Liu, B. Wang, J. Paul Chen and K. Li, *Chem. Commun.*, 2016, **52**, 8869–8872.
- Y.-S. Li, F.-Y. Liang, H. Bux, A. Feldhoff, W.-S. Yang and J. Caro, *Angew. Chem., Int. Ed.*, 2010, **49**, 548–551.
- T. Li, Y. Pan, K.-V. Peinemann and Z. Lai, *J. Membr. Sci.*, 2013, **425–426**, 235–242.
- W. Liang and D. M. D'Alessandro, *Chem. Commun.*, 2013, **49**, 3706–3708.
- W. Liang, C. J. Coghlan, F. Ragon, M. Rubio-Martinez, D. M. D'Alessandro and R. Babarao, *Dalton Trans.*, 2016, **45**, 4496–4500.
- T. Hu, G. Dong, H. Li and V. Chen, *J. Membr. Sci.*, 2014, **468**, 107–117.
- T. Hu, G. Dong, H. Li and V. Chen, *J. Membr. Sci.*, 2013, **432**, 13–24.
- Z. Hu, M. Khurana, Y. H. Seah, M. Zhang, Z. Guo and D. Zhao, *Chem. Eng. Sci.*, 2015, **124**, 61–69.

- 43 G. E. Cmarik, M. Kim, S. M. Cohen and K. S. Walton, *Langmuir*, 2012, **28**, 15606–15613.
- 44 Y. Cao, Y. Zhao, Z. Lv, F. Song and Q. Zhong, *J. Ind. Eng. Chem.*, 2015, **27**, 102–107.
- 45 A. M. Ebrahim and T. J. Bandosz, *ACS Appl. Mater. Interfaces*, 2013, **5**, 10565–10573.
- 46 Z. H. Rada, H. R. Abid, H. Sun and S. Wang, *J. Chem. Eng. Data*, 2015, **60**, 2152–2161.
- 47 Y. Luan, Y. Qi, Z. Jin, X. Peng, H. Gao and G. Wang, *RSC Adv.*, 2015, **5**, 19273–19278.
- 48 Y. Ying, Y. Xiao, J. Ma, X. Guo, H. Huang, Q. Yang, D. Liu and C. Zhong, *RSC Adv.*, 2015, **5**, 28394–28400.
- 49 J. H. Cavka, S. Jakobsen, U. Olsbye, N. Guillou, C. Lamberti, S. Bordiga and K. P. Lillerud, *J. Am. Chem. Soc.*, 2008, **130**, 13850–13851.
- 50 H.-C. Yang, J. Hou, V. Chen and Z.-K. Xu, *J. Mater. Chem. A*, 2016, **4**, 9716–9729.
- 51 S. Lancers-Méndez, J. F. Mano, A. M. Costa and V. H. Schmidt, *J. Macromol. Sci., Part B: Phys.*, 2001, **40**, 517–527.
- 52 A. Ghadimi, T. Mohammadi and N. Kasiri, *Int. J. Hydrogen Energy*, 2015, **40**, 9723–9732.
- 53 H. Rabiee, A. Ghadimi and T. Mohammadi, *J. Membr. Sci.*, 2015, **476**, 286–302.
- 54 V. I. Bondar, B. D. Freeman and I. Pinnau, *J. Polym. Sci., Part B: Polym. Phys.*, 2000, **38**, 2051–2062.
- 55 Y. Wang, H. Li, G. Dong, C. Scholes and V. Chen, *Ind. Eng. Chem. Res.*, 2015, **54**, 7273–7283.
- 56 S. Friebe, B. Geppert, F. Steinbach and J. Caro, *ACS Appl. Mater. Interfaces*, 2017, **9**, 12878–12885.
- 57 A. Bos, I. G. M. Pünt, M. Wessling and H. Strathmann, *J. Membr. Sci.*, 1999, **155**, 67–78.
- 58 A. F. Ismail and W. Lorna, *Sep. Purif. Technol.*, 2002, **27**, 173–194.
- 59 W. Qiu, C.-C. Chen, L. Xu, L. Cui, D. R. Paul and W. J. Koros, *Macromolecules*, 2011, **44**, 6046–6056.
- 60 A. Jomekian, R. M. Behbahani, T. Mohammadi and A. Kargari, *J. Nat. Gas Sci. Eng.*, 2016, **31**, 562–574.
- 61 G. Dong, H. Li and V. Chen, *J. Membr. Sci.*, 2011, **369**, 206–220.
- 62 F. Li, Q. Li, X. Bao, J. Gui and X. Yu, *Korean Chem. Eng. Res.*, 2014, **52**, 340–346.
- 63 A. Halim, Q. Fu, Q. Yong, P. A. Gurr, S. E. Kentish and G. G. Qiao, *J. Mater. Chem. A*, 2014, **2**, 4999–5009.
- 64 Q. Fu, E. H. H. Wong, J. Kim, J. M. P. Scofield, P. A. Gurr, S. E. Kentish and G. G. Qiao, *J. Mater. Chem. A*, 2014, **2**, 17751–17756.
- 65 S. Tan, Q. Fu, J. M. P. Scofield, J. Kim, P. A. Gurr, K. Ladewig, A. Blencowe and G. G. Qiao, *J. Mater. Chem. A*, 2015, **3**, 14876–14886.
- 66 A. K. Zulhairun, Z. G. Fachrurrazi, M. Nur Izwanne and A. F. Ismail, *Sep. Purif. Technol.*, 2015, **146**, 85–93.
- 67 S. Li, Z. Wang, C. Zhang, M. Wang, F. Yuan, J. Wang and S. Wang, *J. Membr. Sci.*, 2013, **436**, 121–131.
- 68 Y. Wang, T. Hu, H. Li, G. Dong, W. Wong and V. Chen, *Energy Procedia*, 2014, **63**, 202–209.

Journal of Materials Chemistry A

Volume 10, Number 1, January 2022



Royal Society of
Chemistry

Journal of
Materials Chemistry A

Volume 10, Number 1, January 2022

Editorial board

Editorial board

Advisory board

Editorial office

Lectureship

Editor-in-chief

[Anders Hagfeldt](#), Uppsala University, Sweden

Associate editors

[Veronica Augustyn](#), North Carolina State University, USA

[Viola Birss](#), University of Calgary, Canada

[Goutam De](#), Satyendra Nath Bose National Centre for Basic Sciences, Kolkata, India

[Mohamed Eddaoudi](#), King Abdullah University of Science and Technology, Saudi Arabia

[Ghim Wei Ho](#), National University of Singapore, Singapore

[Yun Jeong Hwang](#), Seoul National University, South Korea

[Kisuk Kang](#), Seoul National University, South Korea

[David Lou](#), Nanyang Technological University, Singapore

[Yi-Chun Lu](#), The Chinese University of Hong Kong, Hong Kong

[Frank Osterloh](#), University of California, Davis, USA

[Shizhang Qiao](#), University of Adelaide, Australia

[Jennifer Rupp](#), Massachusetts Institute of Technology, USA

[Magdalena Titirici](#), Imperial College London, UK

[Miriam Unterlass](#), University of Konstanz, Germany

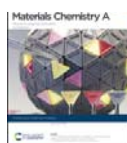
[Li-Zhu Wu](#), Technical Institute of Physics and Chemistry, China

[Yusuke Yamauchi](#), The University of Queensland, Australia

[Zhen Zhou](#), Nankai University, China



Log in / register



Journal of Materials Chemistry A

< [View all journals](#)

Recent

Issues

Collections

[Previous](#)

[Latest](#)

[Next](#)



Journal of Materials Chemistry A

21 January 2018, Issue 3,
Page 683 to 1286

65 items

[Cover info and contents](#)

Review Article

Two- and three-dimensional graphene-based hybrid composites for advanced energy storage and conversion devices

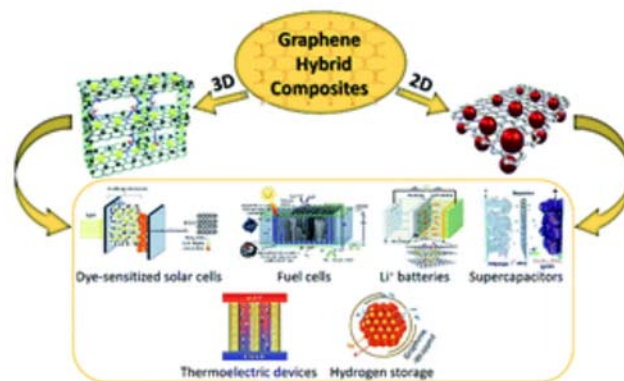
Jalal Azadmanjiri, Vijay K. Srivastava, Parshant Kumar, Mostafa Nikzad, James Wang and Aimin Yu

2D and 3D graphene-based hybrid composites are the most promising materials for a broad range of high-efficiency energy storage and conversion devices.

[Top](#)

[Info](#)

[Search](#)



From the themed collection: [Recent Review Articles](#)

The article was first published on 27 Nov 2017

J. Mater. Chem. A, 2018, **6**, 702-734

<https://doi.org/10.1039/C7TA08748A>

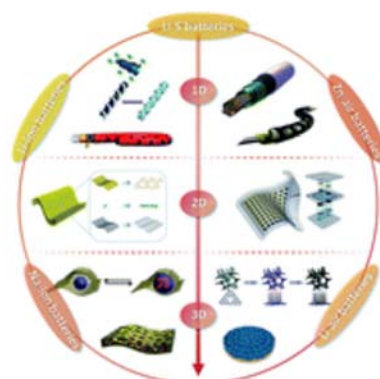
[Download PDF](#) [Article HTML](#)

Review Article

Innovation and challenges in materials design for flexible rechargeable batteries: from 1D to 3D

Yanghua He, Bryan Matthews, Jingyun Wang, Li Song, Xiaoxia Wang and Gang Wu

Due to the emergence of numerous flexible electronic devices, the design and fabrication of flexible rechargeable batteries with high energy density have attracted great attention.



From the themed collection: [Recent Review Articles](#)

[Top](#)

[Info](#)

[Search](#)

[Download PDF](#) [Article HTML](#)

Review Article

Monolithic aerogel photocatalysts: a review

Wenchao Wan, Ruiyang Zhang, Minzhi Ma and Ying Zhou

This review has summarized the recent developments of aerogel photocatalysts along with their fabrication strategies and photocatalytic applications.



From the themed collection: [Recent Review Articles](#)

The article was first published on 12 Dec 2017

J. Mater. Chem. A, 2018, **6**, 754-775

<https://doi.org/10.1039/C7TA09227J>

[Download PDF](#) [Article HTML](#)

Review Article

Electrocatalysis of oxygen reduction on heteroatom-doped nanocarbons and transition metal–nitrogen–carbon catalysts for alkaline membrane fuel cells

Ave Sarapuu, Elo Kibena-Pöldsepp, Maryam Borghei and Kaido Tammeveski

Electrochemical oxygen reduction behaviour and AEMFC performance using non-precious metal cathode catalysts are reviewed.



From the themed collection: [Recent Review Articles](#)

The article was first published on 05 Dec 2017

J. Mater. Chem. A, 2018, **6**, 776-804

<https://doi.org/10.1039/C7TA08690C>

[Download PDF](#) [Article HTML](#)

Communication

Engineering the coordination geometry of metal–organic complex electrocatalysts for highly enhanced oxygen evolution reaction

Dafeng Yan, Chung-Li Dong, Yu-Cheng Huang, Yuqin Zou, Chao Xie, Yanyong Wang, Yiqiong Zhang, Dongdong Liu, Shaohua Shen and Shuangyin Wang

For the first time, we have successfully generated coordinatively unsaturated metal sites in phytic acid–Co²⁺ based metal–organic complexes by engineering the coordination geometry with room-temperature plasma technology.



The article was first published on 05 Dec 2017

J. Mater. Chem. A, 2018, **6**, 805-810

<https://doi.org/10.1039/C7TA09092G>

[Download PDF](#) [Article HTML](#)

[Top](#)

[Info](#)

[Search](#)

Communication

Ti/Co-S catalyst covered amorphous Si-based photocathodes with high photovoltage for the HER in non-acid environments

Qixing Zhang, Tiantian Li, Jingshan Luo, Bofei Liu, Junhui Liang, Ning Wang, Xiangbin Kong, Baozhang Li, Changchun Wei, Ying Zhao and Xiaodan Zhang

Magnetron sputtering and electrochemical-deposition were used to deposit Ti/Co-S catalyst on amorphous Si/amorphous Si tandem solar cells for water-splitting in non-acid solutions.



From the themed collection: [Journal of Materials Chemistry A Advisory Board Collection](#)

The article was first published on 07 Dec 2017

J. Mater. Chem. A, 2018, **6**, 811-816

<https://doi.org/10.1039/C7TA09569D>

[Download PDF](#) [Article HTML](#)

Communication

Evolution of copper oxide nanoneedle mesh with subtle regulated lyophobicity for high efficiency liquid separation

Mengna Qiu, Nü Wang, Zhimin Cui, Jing Liu, Lanlan Hou, Jingchong Liu, Rongjun Hu, Hailong Zhang and Yong Zhao

The relationship between copper oxide nanostructures and lyophobicity has been systematically researched for the design of lyophobic copper materials.



The article was first published on 07 Dec 2017

J. Mater. Chem. A, 2018, **6**, 817-822

<https://doi.org/10.1039/C7TA09217B>

[Download PDF](#) [Article HTML](#)

[Top](#)

[Info](#)

[Search](#)

Radiation-induced grafting of a butyl-spacer styrenic monomer onto ETFE: the synthesis of the most alkali stable radiation-grafted anion-exchange membrane to date

Julia Ponce-González, Imad Ouachan, John R. Varcoe and Daniel K. Whelligan

Adding a butyl spacer between the benzene and *N*-methylpyrrolidinium group led to double the *ex situ* alkaline stability compared to use of a methylene spacer.



From the themed collection: [Recent Open Access Articles](#)

The article was first published on 07 Dec 2017

J. Mater. Chem. A, 2018, **6**, 823-827

<https://doi.org/10.1039/C7TA10222D>

[Download PDF](#) [Article HTML](#)

Communication

Superelastic and ultralight polyimide aerogels as thermal insulators and particulate air filters

Zhenchao Qian, Zhen Wang, Yi Chen, Shengrui Tong, Maofa Ge, Ning Zhao and Jian Xu

Superelasticity, recoverable ultimate strain of 99%, has been obtained for fibrous polyimide aerogels.



The article was first published on 14 Dec 2017

J. Mater. Chem. A, 2018, **6**, 828-832

<https://doi.org/10.1039/C7TA09054D>

[Download PDF](#) [Article HTML](#)

[Top](#)

[Info](#)

[Search](#)

Min Gao, Lanlan Chen, Zhenhua Zhang, Xuping Sun and Shusheng Zhang

It is highly attractive but challenging to design and develop noble-metal-free catalysts with outstanding electrocatalytic activity for the hydrogen evolution reaction (HER) in alkaline media.



The article was first published on 14 Dec 2017

J. Mater. Chem. A, 2018, **6**, 833-836

<https://doi.org/10.1039/C7TA08907D>

[Download PDF](#) [Article HTML](#)

Communication

A small amount of nanoparticulated plant biomass, lignin, enhances the heat tolerance of poly(ethylene carbonate)

K. Shikinaka, H. Sotome, Y. Kubota, Y. Tominaga, M. Nakamura, R. R. Navarro and Y. Otsuka

A small amount of non-deteriorated lignin dramatically enhances the heatproof properties of a synthetic polymer.



The article was first published on 13 Dec 2017

J. Mater. Chem. A, 2018, **6**, 837-839

<https://doi.org/10.1039/C7TA09216D>

[Download PDF](#) [Article HTML](#)

Communication

Aqueous-solution synthesis of Na_3SbS_4 solid electrolytes for all-solid-state Na-ion batteries

Tae Won Kim, Kern Ho Park, Young Eun Choi, Ju Yeon Lee and Yoon Seok Jung

[Top](#)

[Info](#)

[Search](#)



The article was first published on 18 Dec 2017

J. Mater. Chem. A, 2018, **6**, 840-844

<https://doi.org/10.1039/C7TA09242C>

Download PDF Article HTML

Communication

A phenol-formaldehyde polymeric network to generate organic aerogels: synthesis, physicochemical characteristics and potential applications

Halyna Zubyk, Olena Mykhailiv, Anthony N. Papathanassiou, Bogdan Sulikowski, Elzbieta Zambrzycka-Szelewa, Michael Bratychak and Marta E. Plonska-Brzezinska

Two phenol-formaldehyde organic aerogels were prepared and applied for efficient Cu(II) and Mn(II) ion, organic solvent and dye removal from water sources.



The article was first published on 14 Dec 2017

J. Mater. Chem. A, 2018, **6**, 845-852

<https://doi.org/10.1039/C7TA08814K>

Download PDF Article HTML

Communication

3D printing of high performance cyanate ester thermoset polymers

Swetha Chandrasekaran, Eric B. Duoss, Marcus A. Worsley and James P. Lewicki

We report 3D printing of a 'pure' thermal cure cyanate ester for the fabrication of robust 3D printed structures through the formulation, tailoring and post processing of a custom 'ink' for Direct Ink Writing.

Top

Info

Search

The article was first published on 20 Dec 2017

J. Mater. Chem. A, 2018, **6**, 853-858

<https://doi.org/10.1039/C7TA09466C>

[Download PDF](#) [Article HTML](#)

Communication

Nanocasting in ball mills - combining ultra-hydrophilicity and ordered mesoporosity in carbon materials

En Zhang, Guang-Ping Hao, Mirian Elizabeth Casco, Volodymyr Bon, Sven Grätz and Lars Borchardt

Mesoporous carbon with ordered structure and high hydrophilicity is of great interest for many applications. Nanocasting in ball mills opens a pathway to combine the two charming properties by a rapid synthesis of solvent-free N-containing coordination polymer and pyrolysis.



The article was first published on 20 Dec 2017

J. Mater. Chem. A, 2018, **6**, 859-865

<https://doi.org/10.1039/C7TA10783H>

[Download PDF](#) [Article HTML](#)

Communication

Organic-free synthesis and ortho-reaction of monodisperse Ni incorporated CeO₂ nanocatalysts

W. L. Wang, W. Y. Liu, X. L. Weng, Y. Shang, J. J. Chen, Z. G. Chen and Z. B. Wu

Homogeneous solid solutions provide ortho-reaction channels that ensure sufficient contact and reaction of adsorbents and might be very beneficial to Langmuir-Hinshelwood type reactions.



The article was first published on 18 Dec 2017

[Top](#)

[Info](#)

[Search](#)

Download PDF Article HTML

Communication

Efficient removal of aerosol oil-mists using superoleophobic filters

Xin Wei, Feng Chen, Hongxia Wang, Hua Zhou, Zhongli Ji and Tong Lin

Superoleophobic treatment can considerably improve the oil mist filtration performance of glass fibre nonwoven filters.



The article was first published on 21 Dec 2017

J. Mater. Chem. A, 2018, **6**, 871-877

<https://doi.org/10.1039/C7TA10045K>

Download PDF Article HTML

Communication

A phase-transition-assisted method for the rational synthesis of nitrogen-doped hierarchically porous carbon materials for the oxygen reduction reaction

Wei Li, Wei Ding, Jinxia Jiang, Qian He, Sicheng Tao, Wanglan Wang, Jing Li and Zidong Wei

By a novel phase-transition-assisted strategy, the porosity of carbon materials can be fine tuned from the micrometer to the nanometer level, and the functionality of carbon surfaces can be better controlled to achieve an excellent performance for the catalysis of the oxygen reduction reaction.



The article was first published on 11 Dec 2017

J. Mater. Chem. A, 2018, **6**, 878-883

<https://doi.org/10.1039/C7TA09435C>

Top

Info

Search

Paper

Prussian blue analogues derived porous nitrogen-doped carbon microspheres as high-performance metal-free peroxymonosulfate activators for non-radical-dominated degradation of organic pollutants

Na Wang, Wenjie Ma, Ziqiu Ren, Yunchen Du, Ping Xu and Xijiang Han

Herein, Zn–Co Prussian blue analogues derived porous nitrogen-doped carbon are applied for the degradation of organic pollutants *via* a non-radical pathway.



The article was first published on 14 Nov 2017

J. Mater. Chem. A, 2018, **6**, 884–895

<https://doi.org/10.1039/C7TA08472B>

Download PDF Article HTML

Paper

Hierarchically porous sheath–core graphene-based fiber-shaped supercapacitors with high energy density

Xianhong Zheng, Kun Zhang, Lan Yao, Yiping Qiu and Shiren Wang

Hierarchically porous, micropore-domain graphene-based fiber-shaped supercapacitors show high energy density.



The article was first published on 06 Nov 2017

J. Mater. Chem. A, 2018, **6**, 896–907

<https://doi.org/10.1039/C7TA08362A>

Download PDF Article HTML

Top

Info

Search

graphene through rotary plasma processing

Jinghuang Lin, Henan Jia, Yifei Cai, Shulin Chen, Haoyan Liang, Xu Wang, Fu Zhang, Junlei Qi, Jian Cao, Jikai Feng and Wei-dong Fei

We strategically created defects on the side surfaces of VFG *via* defect engineering using rotary plasma etching, which not only improves the wettability with electrolyte, but also provides more electroactive sites.



The article was first published on 03 Nov 2017

J. Mater. Chem. A, 2018, **6**, 908-917

<https://doi.org/10.1039/C7TA06490J>

Download PDF Article HTML

Paper

Surface functionalized UiO-66/Pebax-based ultrathin composite hollow fiber gas separation membranes

Putu Doddy Sutrisna, Jingwei Hou, Muhammad Yazid Zulkifli, Hongyu Li, Yatao Zhang, Weibin Liang, Deanna M. D'Alessandro and Vicki Chen

Pebax-based composite hollow fiber membranes are fabricated with functionalized MOFs, and the effect of MOF rigidity is discussed.



The article was first published on 02 Nov 2017

J. Mater. Chem. A, 2018, **6**, 918-931

<https://doi.org/10.1039/C7TA07512J>

Download PDF Article HTML

Paper

Top

Info

Search

With increased charge carrier density and efficient CO₂ activation, the MOF-based hybrid ternary nanocomposite exhibits a high CO₂ conversion efficiency and preferential formation of CH₄.



The article was first published on 05 Dec 2017

J. Mater. Chem. A, 2018, **6**, 932-940

<https://doi.org/10.1039/C7TA09192C>

[Download PDF](#) [Article HTML](#)

Paper

Ag-Doped PEDOT:PSS/CNT composites for thin-film all-solid-state supercapacitors with a stretchability of 480%

Yaping Zhu, Ning Li, Tian Lv, Yao Yao, Huanan Peng, Jun Shi, Shaokui Cao and Tao Chen

A highly flexible and stretchable all-solid-state supercapacitor that can bear a tensile strain as high as 480% is developed by using composite electrodes of aligned carbon nanotube and silver-doped poly(3,4-ethylenedioxythiophene)-poly(styrenesulfonate).



The article was first published on 30 Nov 2017

J. Mater. Chem. A, 2018, **6**, 941-947

<https://doi.org/10.1039/C7TA09154K>

[Download PDF](#) [Article HTML](#)

Paper

Rational design of asymmetric benzodithiophene based photovoltaic polymers for efficient solar cells

Tingting Zhu, Deyu Liu, Kaili Zhang, Yonghai Li, Zhe Liu, Xudong Gao, Xichang Bao, Mingliang Sun and Renqiang Yang

[Top](#)

[Info](#)

[Search](#)



The article was first published on 30 Nov 2017

J. Mater. Chem. A, 2018, **6**, 948-956

<https://doi.org/10.1039/C7TA09736K>

[Download PDF](#) [Article HTML](#)

Paper

Improved photocurrent and efficiency of non-fullerene organic solar cells despite higher charge recombination

Biao Xiao, Jingnan Song, Bing Guo, Minli Zhang, Wanbin Li, Ruixue Zhou, Jiyan Liu, Hong-Bo Wang, Maojie Zhang, Guoping Luo, Feng Liu and Thomas P. Russell

Charge recombination in high-efficiency non-fullerene cells (PCE = 9.25%) is much more serious than that of fullerene based cells (PCE = 6.95%).



The article was first published on 04 Dec 2017

J. Mater. Chem. A, 2018, **6**, 957-962

<https://doi.org/10.1039/C7TA07501D>

[Download PDF](#) [Article HTML](#)

Paper

A facile nanocomposite strategy to fabricate a rGO-MWCNT photothermal layer for efficient water evaporation

Yuchao Wang, Canzhu Wang, Xiangju Song, Suresh Kumar Megarajan and Heqing Jiang

A facile strategy based on a nanocomposite is developed to fabricate a rGO-MWCNT membrane for the improvement of photothermal evaporation.

[Top](#)

[Info](#)

[Search](#)

The article was first published on 30 Nov 2017

J. Mater. Chem. A, 2018, **6**, 963-971

<https://doi.org/10.1039/C7TA08972D>

Download PDF Article HTML

Paper

***In situ* g-C₃N₄ self-sacrificial synthesis of a g-C₃N₄/LaCO₃OH heterostructure with strong interfacial charge transfer and separation for photocatalytic NO removal**

Zhenyu Wang, Yu Huang, Long Chen, Meijuan Chen, Junji Cao, Wingkei Ho and Shun Cheng Lee

A novel g-C₃N₄/LaCO₃OH heterojunction was controllably fabricated *via* an *in situ* self-sacrificial strategy and this strategy was extended to synthesize g-C₃N₄/carbonate compounds.



From the themed collection: [2018 Journal of Materials Chemistry A HOT Papers](#)

The article was first published on 01 Dec 2017

J. Mater. Chem. A, 2018, **6**, 972-981

<https://doi.org/10.1039/C7TA09132J>

Download PDF Article HTML

Paper

Laser co-ablation of bismuth antimony telluride and diamond-like carbon nanocomposites for enhanced thermoelectric performance

Tsung-Han Chen, Po-Hung Chen and Chun-Hua Chen

A series of innovative heterogeneous nanocomposites comprising diamond-like carbon (DLC) clusters and well-aligned Bi-Sb-Te based nanoassemblies were realized for thermoelectric enhancement.



Top

Info

Search

<https://doi.org/10.1039/C7TA08701B>

[Download PDF](#) [Article HTML](#)

Paper

Carboxylated polyimide separator with excellent lithium ion transport properties for a high-power density lithium-ion battery

Chun-Er Lin, Hong Zhang, You-Zhi Song, Yin Zhang, Jia-Jia Yuan and Bao-Ku Zhu

Carboxyl groups on the separator improve the lithium ion transport rate by 6 times in the lithium ion battery.



The article was first published on 05 Dec 2017

J. Mater. Chem. A, 2018, **6**, 991-998

<https://doi.org/10.1039/C7TA08702K>

[Download PDF](#) [Article HTML](#)

Paper

Synthesis of $\text{Cu}_2(\text{Zn}_{1-x}\text{Co}_x)\text{SnS}_4$ nanocrystals and formation of polycrystalline thin films from their aqueous dispersions

Alexandre H. Pinto, Seung Wook Shin, Aastha Sharma, R. Lee Penn and Eray S. Aydil

$\text{Cu}_2(\text{Zn}_{1-x}\text{Co}_x)\text{SnS}_4$ nanocrystals were synthesized using a microwave solvothermal method. The influence of Co incorporation in the annealed thin films formation was analyzed.



The article was first published on 20 Dec 2017

J. Mater. Chem. A, 2018, **6**, 999-1008

<https://doi.org/10.1039/C7TA06295H>

[Top](#)

[Info](#)

[Search](#)

Paper

Low toxicity environmentally friendly single component aqueous organic ionic conductors for high efficiency photoelectrochemical solar cells

Jayraj V. Vaghasiya, Dilip Krishna Nandakumar, Zhang Yaoxin and Swee Ching Tan

Low-toxic, environment friendly single component organic ionic conductors are synthesized by facile methods and used as electrolytes in Dye Sensitized Solar Cells (DSSCs).



The article was first published on 08 Dec 2017

J. Mater. Chem. A, 2018, **6**, 1009-1016

<https://doi.org/10.1039/C7TA09557K>

Download PDF Article HTML

Paper

Graphene-coupled Ti_3C_2 MXenes-derived TiO_2 mesostructure: promising sodium-ion capacitor anode with fast ion storage and long-term cycling

Rutao Wang, Shijie Wang, Yabin Zhang, Dongdong Jin, Xinyong Tao and Li Zhang

Graphene coupled Ti_3C_2 MXenes-derived TiO_2 mesostructure with robust Na-ion charge storage properties enables the fabrication of high-performance Na-ion capacitors.



The article was first published on 12 Dec 2017

J. Mater. Chem. A, 2018, **6**, 1017-1027

<https://doi.org/10.1039/C7TA09153B>

Download PDF Article HTML

Top

Info

Search

rate performance

Seung-Keun Park, Jin-Sung Park and Yun Chan Kang

Novel porous carbon nanofibers with bimodal pores were synthesized by carbonization of electrospun zeolitic imidazole framework-8/polyacrylonitrile nanofibers and further chemical activation.

The article was first published on 08 Dec 2017

J. Mater. Chem. A, 2018, **6**, 1028-1036

<https://doi.org/10.1039/C7TA09676C>

Download PDF Article HTML

Paper

Effect of tantalum doping in a TiO₂ compact layer on the performance of planar spiro-OMeTAD free perovskite solar cells

Rahul Ranjan, Asit Prakash, Arjun Singh, Anand Singh, Ashish Garg and Raju Kumar Gupta

This work investigates the effect of tantalum doping in compact TiO₂ layer on the performance of planar spiro-OMeTAD free perovskite solar cells. 40% improvement in the overall efficiency was obtained as compared to the device with undoped TiO₂.

The article was first published on 07 Dec 2017

J. Mater. Chem. A, 2018, **6**, 1037-1047

<https://doi.org/10.1039/C7TA09193A>

Download PDF Article HTML

Paper

Top

Info

Search

In this work, $\text{CoMoO}_4/\text{Co}_3\text{O}_4$ hollow porous octahedrons are synthesized by thermal conversion of a cyanide-metal framework (CMF) compound of $\text{Co}_2[\text{Mo}(\text{CN})_8] \cdot x\text{H}_2\text{O}$.



The article was first published on 08 Dec 2017

J. Mater. Chem. A, 2018, **6**, 1048-1056

<https://doi.org/10.1039/C7TA08868J>

[Download PDF](#) [Article HTML](#)

Paper

Red-blood-cell-like $(\text{NH}_4)[\text{Fe}_2(\text{OH})(\text{PO}_4)_2] \cdot 2\text{H}_2\text{O}$ particles: fabrication and application in high-performance LiFePO_4 cathode materials

Kaipeng Wu, Ke Du and Guorong Hu

Red-blood-cell-like $(\text{NH}_4)[\text{Fe}_2(\text{OH})(\text{PO}_4)_2] \cdot 2\text{H}_2\text{O}$, synthesized by a facile sonochemical method, has been used as a valuable precursor to fabricate high performance LiFePO_4/C .



The article was first published on 18 Oct 2017

J. Mater. Chem. A, 2018, **6**, 1057-1066

<https://doi.org/10.1039/C7TA08413G>

[Download PDF](#) [Article HTML](#)

Paper

Influence of water intercalation and hydration on chemical decomposition and ion transport in methylammonium lead halide perovskites

Un-Gi Jong, Chol-Jun Yu, Gum-Chol Ri, Andrew P. McMahon, Nicholas M. Harrison, Piers R. F. Barnes and Aron Walsh

The application of methylammonium (MA) lead halide perovskites, $\text{CH}_3\text{NH}_3\text{PbX}_3$ ($X = \text{I}, \text{Br}, \text{Cl}$), in

[Top](#)

[Info](#)

[Search](#)



From the themed collection: [Recent Open Access Articles](#)

The article was first published on 05 Dec 2017

J. Mater. Chem. A, 2018, **6**, 1067-1074

<https://doi.org/10.1039/C7TA09112E>

[Download PDF](#) [Article HTML](#)

Paper

CoS₂-TiO₂ hybrid nanostructures: efficient and durable bifunctional electrocatalysts for alkaline electrolyte membrane water electrolyzers

Pandian Ganesan, Arumugam Sivanantham and Sangaraju Shanmugam

The TiO₂ supported Co(TU)-derived CoS₂ nanostructures show remarkable bifunctional electrochemical activity and ultra-stability in alkaline electrolyte membrane water electrolysis.



The article was first published on 08 Dec 2017

J. Mater. Chem. A, 2018, **6**, 1075-1085

<https://doi.org/10.1039/C7TA09096J>

[Download PDF](#) [Article HTML](#)

Paper

CuGaS₂ nanoplates: a robust and self-healing anode for Li/Na ion batteries in a wide temperature range of 268–318 K

Yun Song, Yanmei Li, Lin Zhu, Zhichang Pan, Yinchang Jiang, Pei Wang, Yong-Ning Zhou, Fang Fang, Linfeng Hu and Dalin Sun

CuGaS₂ hexagonal nanoplates were found to be a novel and robust anode material in a wide temperature range.

[Top](#)

[Info](#)

[Search](#)

The article was first published on 06 Dec 2017

J. Mater. Chem. A, 2018, **6**, 1086-1093

<https://doi.org/10.1039/C7TA09197D>

[Download PDF](#) [Article HTML](#)

 Paper

Towards centimeter thick transparent wood through interface manipulation

Yuanyuan Li, Xuan Yang, Qiliang Fu, Ramiro Rojas, Min Yan and Lars Berglund

A centimeter-thick transparent wood structure was realized through interface manipulation.



From the themed collection: [Recent Open Access Articles](#)

The article was first published on 13 Dec 2017

J. Mater. Chem. A, 2018, **6**, 1094-1101

<https://doi.org/10.1039/C7TA09973H>

[Download PDF](#) [Article HTML](#)

Paper

Cyclodextrin-gold nanocluster decorated TiO₂ enhances photocatalytic decomposition of organic pollutants

Haiguang Zhu, Nirmal Goswami, Qiaofeng Yao, Tiankai Chen, Yanbiao Liu, Qingfeng Xu, Dongyun Chen, Jianmei Lu and Jianping Xie

We decorated per-6-thio-β-cyclodextrin protected gold nanoclusters on TiO₂ nanoparticles to improve photocatalytic activity by inhibiting electron-hole pair recombination and absorbing organic targets *via* host-guest interactions.



[Top](#)

[Info](#)

[Search](#)

[Download PDF](#) [Article HTML](#)

Paper

A true cable assembly with a carbon nanotube sheath and nickel wire core: a fully flexible electrode integrating energy storage and electrical conduction

Huating Ye, Kai Wang, Juntao Zhou, Li Song, Li Gu and Xuebo Cao

Scalable production of fully flexible cables consisting of a carbon nanotube sheath and nickel wire core for wire-shaped supercapacitors is demonstrated.



The article was first published on 12 Dec 2017

J. Mater. Chem. A, 2018, **6**, 1109-1118

<https://doi.org/10.1039/C7TA08758F>

[Download PDF](#) [Article HTML](#)

Paper

Monolithic mesoporous graphitic composites as super capacitors: from Starbons to Starenes®

Andrea Muñoz García, Vitaliy L. Budarin, Yixin Zhou, Mario De bruyn, Andrew J. Hunt, Leonardo Lari, Vlado K. Lazarov, Horacio J. Salavagione, Enrique Morales, Gary J. Ellis, James H. Clark and Peter S. Shuttleworth

Sustainable electric double-layer capacitor (EDLC) electrodes were made by incorporating nanographite particles into the electrode pore walls, improving conductivity and capacitance. The combination of ball milling, microwave processing and carbonisation were key to excellent nanoparticle dispersion.



The article was first published on 18 Dec 2017

J. Mater. Chem. A, 2018, **6**, 1119-1127

[Top](#)

[Info](#)

[Search](#)

[Download PDF](#) [Article HTML](#)

Paper

Lithium-ion intercalation and deintercalation behaviors of graphitized carbon nanospheres

Shohei Maruyama, Tomokazu Fukutsuka, Kohei Miyazaki, Yumi Abe, Noriko Yoshizawa and Takeshi Abe

The electrochemical properties of graphitized carbon nanospheres as a promising negative electrode material for high-rate lithium-ion batteries were correlated with lithium-ion intercalation and deintercalation behaviors.



The article was first published on 22 Dec 2017

J. Mater. Chem. A, 2018, **6**, 1128-1137

<https://doi.org/10.1039/C7TA07902H>

[Download PDF](#) [Article HTML](#)

[Top](#)

[Info](#)

[Search](#)

Paper

Simple combination of a protic salt and an iron halide: precursor for a Fe, N and S co-doped catalyst for the oxygen reduction reaction in alkaline and acidic media

Mahfuzul Hoque, Shiguo Zhang, Morgan L. Thomas, Zhe Li, Soma Suzuki, Ayumi Ando, Masato Yanagi, Yoshio Kobayashi, Kaoru Dokko and Masayoshi Watanabe

A simple and robust strategy for an Fe based oxygen reduction catalyst using a protic salt and an iron halide.



The article was first published on 11 Dec 2017

J. Mater. Chem. A, 2018, **6**, 1138-1149

<https://doi.org/10.1039/C7TA09975D>

Download PDF Article HTML

Paper

Bulk properties and transport mechanisms of a solid state antiperovskite Li-ion conductor Li₃OCl: insights from first principles calculations

Musheng Wu, Bo Xu, Xueling Lei, Kelvin Huang and Chuying Ouyang

Systematic study on bulk properties, defect chemistry and Li-ion transport mechanisms of a Li₃OCl fast-ion conductor.



The article was first published on 08 Dec 2017

J. Mater. Chem. A, 2018, **6**, 1150-1160

<https://doi.org/10.1039/C7TA08780B>

Download PDF Article HTML

Top

Info

Search

Cong-Cong Zhang, Zhao-Kui Wang, Meng Li, Zhi-Yong Liu, Ji-En Yang, Ying-Guo Yang, Xing-Yu Gao and Heng Ma

We develop an external-electric-field (EEF)-assisted annealing treatment to improve the photoelectric performance of planar organic–inorganic perovskite solar cells (PSCs).



The article was first published on 08 Dec 2017

J. Mater. Chem. A, 2018, **6**, 1161-1170

<https://doi.org/10.1039/C7TA08204E>

[Download PDF](#) [Article HTML](#)

Paper

Tuning the structural stability of LiBH_4 through boron-based compounds towards superior dehydrogenation

Weitong Cai, Juner Chen, Liying Liu, Yuanzheng Yang and Hui Wang

A $\text{LiBH}_4\text{-H}_3\text{BO}_3$ destabilization system shows significantly lower temperature, rapid kinetics, pure hydrogen and high capacity through $[\text{BH}_4]^- \cdots [\text{OH}]^-$ interaction.



The article was first published on 11 Dec 2017

J. Mater. Chem. A, 2018, **6**, 1171-1180

<https://doi.org/10.1039/C7TA09376D>

[Download PDF](#) [Article HTML](#)

Paper

Controlling interpenetration through linker conformation in the modulated synthesis of Sc metal-organic frameworks

Ross J. Marshall, Ciaran T. Lennon, Andi Tao, Hans M. Senn, Claire Wilson, David Fairen-Jimenez and Ross S. Forgan

[Top](#)

[Info](#)

[Search](#)

From the themed collection: [Recent Open Access Articles](#)

The article was first published on 15 Dec 2017

J. Mater. Chem. A, 2018, **6**, 1181-1187

<https://doi.org/10.1039/C7TA09699B>

[Download PDF](#) [Article HTML](#)

Paper

A novel two-dimensional nickel phthalocyanine-based metal-organic framework for highly efficient water oxidation catalysis

Hongxing Jia, Yuchuan Yao, Jiangtao Zhao, Yuyue Gao, Zhenlin Luo and Pingwu Du

For the first time, we report herein bottom-up fabrication of a conductive nickel phthalocyanine-based 2D MOF and use it as a highly active electrocatalyst for OER (overpotential < 250 mV) without further pyrolysis or adding conductive materials, which can facilitate the development of 2D MOFs for energy applications.

The article was first published on 12 Dec 2017

J. Mater. Chem. A, 2018, **6**, 1188-1195

<https://doi.org/10.1039/C7TA07978H>

[Download PDF](#) [Article HTML](#)

Paper

Rapid and facile synthesis of hierarchically mesoporous TiO₂-B with enhanced reversible capacity and rate capability

Yubin Liu, Minghuang Guo, Zhenwei Liu, Qiaohua Wei and Mingdeng Wei

A rapid and facile synthetic route has been developed to fabricate hierarchically mesoporous

[Top](#)

[Info](#)

[Search](#)



The article was first published on 15 Dec 2017

J. Mater. Chem. A, 2018, **6**, 1196-1200

<https://doi.org/10.1039/C7TA09264D>

[Download PDF](#) [Article HTML](#)

Paper

Enhancing oxygen permeation through $\text{Fe}_2\text{NiO}_4\text{-Ce}_{0.8}\text{Tb}_{0.2}\text{O}_{2-\delta}$ composite membranes using porous layers activated with Pr_6O_{11} nanoparticles

Julio García-Fayos, Rian Ruhl, Laura Navarrete, Henny J. M. Bouwmeester and Jose M. Serra

$\text{Fe}_2\text{NiO}_4\text{-Ce}_{0.8}\text{Tb}_{0.2}\text{O}_{2-\delta}$ (NFO-CTO) composite membranes are of interest to separate oxygen from air.



The article was first published on 12 Dec 2017

J. Mater. Chem. A, 2018, **6**, 1201-1209

<https://doi.org/10.1039/C7TA06485C>

[Download PDF](#) [Article HTML](#)

Paper

Highly ordered $\text{ZnO}/\text{ZnFe}_2\text{O}_4$ inverse opals with binder-free heterojunction interfaces for high-performance photoelectrochemical water splitting

Tingting Yang, Jiawei Xue, Hao Tan, Anjian Xie, Shikuo Li, Wensheng Yan and Yuhua Shen

Highly ordered macroporous $\text{ZnO}/\text{ZnFe}_2\text{O}_4$ inverse opals with binder-free heterojunction interfaces improve the separation of photogenerated charge carriers for high-performance PEC water splitting.

[Top](#)

[Info](#)

[Search](#)

The article was first published on 11 Dec 2017

J. Mater. Chem. A, 2018, **6**, 1210-1218

<https://doi.org/10.1039/C7TA07798J>

[Download PDF](#) [Article HTML](#)

Paper

Phosphorus functionalization for the rapid preparation of highly nanoporous submicron-diameter carbon fibers by electrospinning of lignin solutions

F. J. García-Mateos, R. Berenguer, M. J. Valero-Romero, J. Rodríguez-Mirasol and T. Cordero

Rapid preparation of low-cost carbon fibers by electrospinning of lignin solutions thanks to the functionalization with H₃PO₄.



From the themed collection: [2018 Journal of Materials Chemistry A HOT Papers](#)

The article was first published on 13 Dec 2017

J. Mater. Chem. A, 2018, **6**, 1219-1233

<https://doi.org/10.1039/C7TA08788H>

[Download PDF](#) [Article HTML](#)

Paper

Improved sodium-ion storage performance of Ti₃C₂T_x MXenes by sulfur doping

Jiabao Li, Dong Yan, Shujin Hou, Yuquan Li, Ting Lu, Yefeng Yao and Likun Pan

A S-doped Ti₃C₂T_x MXene was synthesized and applied as an anode material for sodium-ion batteries for the first time.



The article was first published on 15 Dec 2017

[Top](#)

[Info](#)

[Search](#)

[Download PDF](#) [Article HTML](#)

Paper

A green and scalable route to yield porous carbon sheets from biomass for supercapacitors with high capacity

Cunjing Wang, Dapeng Wu, Hongju Wang, Zhiyong Gao, Fang Xu and Kai Jiang

A green route is developed to prepare hierarchical porous carbon sheets (HPCS) from biomass directly under air atmosphere without inert gas protection. The as-prepared HPCS with ultra-thin structure, rich O doping sites and large SSA demonstrate excellent specific capacitance and stability when used in supercapacitor.



The article was first published on 13 Dec 2017

J. Mater. Chem. A, 2018, **6**, 1244-1254

<https://doi.org/10.1039/C7TA07579K>

[Download PDF](#) [Article HTML](#)

Paper

Systematic structure control of ammonium iodide salts as feasible UCST-type forward osmosis draw solutes for the treatment of wastewater

Jeongseon Park, Heeyoung Joo, Minwoo Noh, Yon Namkoong, Seonju Lee, Kyung Hwa Jung, Hye Ryun Ahn, Seulah Kim, Jong-Chan Lee, Jae Hoon Yoon and Yan Lee

Systematic structure control of ammonium iodide salts is designed using novel UCST-type forward osmosis draw solutes for wastewater treatment.



The article was first published on 11 Dec 2017

J. Mater. Chem. A, 2018, **6**, 1255-1265

[Top](#)

[Info](#)

[Search](#)

[Download PDF](#) [Article HTML](#)

Paper

A precious metal-free solar water splitting cell with a bifunctional cobalt phosphide electrocatalyst and doubly promoted bismuth vanadate photoanode

Jin Hyun Kim, Suenghoon Han, Yim Hyun Jo, Yunji Bak and Jae Sung Lee

A bifunctional cobalt phosphide (CoP) electrocatalyst is applied to a doubly promoted BiVO₄ photoanode as an oxygen evolution as well as to a cathode as a hydrogen evolution reaction (HER) catalyst to establish a photoelectrochemical (PEC) water splitting cell made of only earth abundant elements without any precious metals.



The article was first published on 13 Dec 2017

J. Mater. Chem. A, 2018, **6**, 1266-1274

<https://doi.org/10.1039/C7TA09134F>

[Download PDF](#) [Article HTML](#)

Paper

Glutathione-coated Fe₃O₄ nanoparticles with enhanced Fenton-like activity at neutral pH for degrading 2,4-dichlorophenol

Rui Zhou, Ningfei Shen, Jian Zhao, Yu Su and Hejun Ren

Fe₃O₄@GSH nanoparticles exhibit a strong affinity for H₂O₂ under neutral pH conditions.



The article was first published on 14 Dec 2017

J. Mater. Chem. A, 2018, **6**, 1275-1283

<https://doi.org/10.1039/C7TA09685B>

[Top](#)

[Info](#)

[Search](#)




Ads by Google

[Stop seeing this ad](#)
[Why this ad? ⓘ](#)

Journal of Materials Chemistry A

COUNTRY

United Kingdom


 Universities and research institutions in United Kingdom

SUBJECT AREA AND CATEGORY

Chemistry
Chemistry (miscellaneous)

Energy
Renewable Energy, Sustainability and the Environment

Materials Science
Materials Science (miscellaneous)

PUBLISHER

Royal Society of Chemistry

H-INDEX

212

PUBLICATION TYPE

Journals

ISSN

20507488, 20507496

COVERAGE

2013-2020

INFORMATION

[Homepage](#)

[How to publish in this journal](#)

[Contact](#)

SCOPE

Journal of Materials Chemistry A, B & C cover high quality studies across all fields of materials chemistry. The journals focus on those theoretical or experimental studies that report new understanding, applications, properties and synthesis of materials. The journals have a strong history of publishing quality reports of interest to interdisciplinary communities and providing an efficient and rigorous service through peer review and publication. The journals are led by an international team of Editors-in-Chief and Associate Editors who are all active researchers in their fields. Journal of Materials Chemistry A, B & C are separated by the intended application of the material studied. Broadly, applications in energy and sustainability are of interest to Journal of Materials Chemistry A [...]. Example topic areas within the scope of Journal of Materials Chemistry A are listed below. This list is neither exhaustive nor exclusive. Artificial photosynthesis, Batteries, Carbon dioxide conversion, Catalysis, Fuel cells, Gas capture/separation/storage, Green/sustainable materials, Hydrogen generation, Hydrogen storage, Photocatalysis, Photovoltaics, Self-cleaning materials, Self-healing materials, Sensors, Supercapacitors, Thermoelectrics, Water splitting, Water treatment

 Join the conversation about this journal

 Quartiles


FIND SIMILAR JOURNALS ⓘ

options ⋮

Rank	Journal Name	Country	Similarity
1	Materials Today Energy	GBR	94%
2	ACS Applied Energy Materials	USA	92%
3	Advanced Energy Materials	DEU	88%
4	Journal of Energy Chemistry	NLD	85%
5	Nano-Micro Letters	NLD	84%





← Show this widget in your own website
Just copy the code below and paste within your html code:
``

SCImago Graphica

Explore, visually communicate and make sense of data with our new free tool.

Get it



Metrics based on Scopus® data as of April 2021

S **Shahid** 3 months ago

Does Journal of Materials Chemistry A is gold or green open access journal?

reply

SCImago Team



Melanie Ortiz 2 months ago

Dear Shahid,
Thank you for contacting us.
We suggest you visit the journal's homepage or contact the journal's editorial staff, so they could inform you more deeply.
Best Regards, SCImago Team

Y **Yuvraj Sahu** 2 years ago

Hello and Good Morning .My research area is alkaline oxidation of penicillanic acid derivatives. May I publish my original research work in your highly reputed journal? Would you mind helping me ? I expect positively.

Hoping your stay be safe and fine during this pandemic situation.

reply

SCImago Team



Melanie Ortiz 2 years ago

Dear Yuvraj,
thank you for contacting us.
We are sorry to tell you that SCImago Journal & Country Rank is not a journal. SJR is a portal with scientometric indicators of journals indexed in Elsevier/Scopus. Unfortunately, we cannot help you with your request, we suggest you visit the journal's homepage (See submission/author guidelines) or contact the journal's editorial staff, so they could inform you more deeply.

Best Regards, SCImago Team

D **dereje fedasa** 2 years ago

how are you?

reply

R **Riyadi Juhana** 2 years ago

submitte og journal

reply



Melanie Ortiz 2 years ago

SCImago Team

Dear Riyadi, thank you very much for your comment, we suggest you to look for author's instructions/submission guidelines in the journal's website. Best Regards, SCImago Team

Leave a comment

Name

Email

(will not be published)

Submit

The users of Scimago Journal & Country Rank have the possibility to dialogue through comments linked to a specific journal. The purpose is to have a forum in which general doubts about the processes of publication in the journal, experiences and other issues derived from the publication of papers are resolved. For topics on particular articles, maintain the dialogue through the usual channels with your editor.

Developed by:

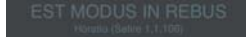


Powered by:



Follow us on @ScimagoJR

Scimago Lab, Copyright 2007-2020. Data Source: Scopus®





Source details

Journal of Materials Chemistry A

Formerly part of: Journal of Materials Chemistry

Scopus coverage years: from 2013 to Present

Publisher: Royal Society of Chemistry

ISSN: 2050-7488 E-ISSN: 2050-7496

Subject area: Materials Science: General Materials Science Chemistry: General Chemistry

Energy: Renewable Energy, Sustainability and the Environment

Source type: Journal

CiteScore 2020

19.7



SJR 2020

3.637



SNIP 2020

1.668



[View all documents >](#)

[Set document alert](#)

[Save to source list](#)

[CiteScore](#) [CiteScore rank & trend](#) [Scopus content coverage](#)

CiteScore 2020 ▼

$$19.7 = \frac{199,466 \text{ Citations } 2017 - 2020}{10,114 \text{ Documents } 2017 - 2020}$$

Calculated on 05 May, 2021

CiteScoreTracker 2021 ⓘ

$$21.0 = \frac{203,774 \text{ Citations to date}}{9,713 \text{ Documents to date}}$$

Last updated on 06 March, 2022 • Updated monthly

CiteScore rank 2020 ⓘ

Category	Rank	Percentile
Materials Science		
General Materials Science	#15/455	96th
Chemistry		
General Chemistry	#15/398	96th
Energy		
Renewable Energy, Sustainability and the Environment	#8/195	96th

[View CiteScore methodology >](#) [CiteScore FAQ >](#) [Add CiteScore to your site](#)

About Scopus

- [What is Scopus](#)
- [Content coverage](#)
- [Scopus blog](#)
- [Scopus API](#)
- [Privacy matters](#)

Language

- [日本語に切り替える](#)
- [切换到简体中文](#)
- [切换到繁體中文](#)
- [Русский язык](#)

Customer Service

- [Help](#)
- [Tutorials](#)
- [Contact us](#)

ELSEVIER

[Terms and conditions](#) ↗ [Privacy policy](#) ↗

Copyright © Elsevier B.V. ↗. All rights reserved. Scopus® is a registered trademark of Elsevier B.V.

We use cookies to help provide and enhance our service and tailor content. By continuing, you agree to the use of cookies.

